International Journal of Speleology	53 (2)	169-190	Tampa, FL (USA)	June 2024

Available online at scholarcommons.usf.edu/ijs

International Journal of Speleology

Official Journal of Union Internationale de Spéléologie

Constraining the evolutionary stages of a hypogene karst system by combining morphological, geochemical and geochronological data - the example of carbonate breccia-hosted Melnička Peštera

Marjan Temovski [1,2,*], Zsófia Ruszkiczay-Rüdiger [3,4], Kata Molnár [1], László Rinyu [1], Alexander Wieser [5], Oscar Marchhart [5], and László Palcsu[1]

[1]HUN-REN Institute for Nuclear Research (ATOMKI), Bem tér 18/c, 4026 Debrecen, Hungary
[2]Department of Mineralogy and Geology, University of Debrecen, Egyetem tér 1, 4032 Debrecen, Hungary
[3]Institute for Geological and Geochemical Research, HUN-REN Research Centre for Astronomy and Earth Sciences, Budaörsi út 45, 1112 Budapest, Hungary
[4]CSFK, MTA Centre of Excellence, Konkoly Thege Miklós út 15-17, 1121 Budapest, Hungary
[5]University of Vienna, Faculty of Physics - Isotope Physics, Waehringer Strasse 17, 1090 Vienna, Austria

Abstract: A combination of morphological observations, geochemical data from calcite minerals and geochronology by burial age dating and U-series is used to constrain the geological and geomorphological setting and the evolutionary stages of a hypogene karst system. This methodological suit is applied to Melnička Peštera, a horizontal cave developed in carbonate breccia overlying dolomite marble in Melnica locality (N. Macedonia), where hydrothermal karst development occurred in both dolomite and calcite marble. The passage morphology of the cave, having a reverse triangle, Laughöhle cross-sections, suggests development near the water table by slowly moving waters. Calcite crusts are found throughout the cave, and based on their relationship to passage morphology, appear to pre-date main horizontal passage formation. Their carbonate stable and clumped isotope and fluid inclusion noble gas compositions indicate cooling of the hydrothermal system with an increased contribution of shallower groundwater. U-series data suggests Early Pleistocene deposition of the calcite crusts. Water table notches and convectional features carved into breccia bedrock and calcite crusts point to subsequent development at and above the water table by condensation corrosion. The solutional aggressiveness near the water table was likely related to CO_2, that previously degassed from the deeper parts of the system where calcite was depositing, and redissolved in the cooler, shallower waters. Due to poor connection with the surface, the cave air above the water table likely had high pCO_2, that further helped to maintain aggressiveness of the groundwater at the water-air contact, and boosted condensation corrosion above it, preventing deposition of related secondary calcite minerals. The cave-hosting carbonate breccia deposited as an alluvial fan filling up a paleovalley cut into Upper Miocene sediments. Cosmogenic nuclide burial age dating of quartz fragments confirms Early Pliocene age for the breccia, and constrains the paleovalley incision to Late Miocene, likely related to base level lowering caused by the Messinian Salinity Crisis.

Keywords: hydrothermal speleogenesis, stable isotopes, noble gases, burial age dating, Mariovo

Received 28 March 2024; Revised 14 July 2024; Accepted 17 July 2024

Citation: Temovski, M., Ruszkiczay-Rüdiger, Z., Molnár, K., Rinyu, L., Wieser, A., Marchhart, O., Palcsu, L., 2024. Constraining the evolutionary stages of a hypogene karst system by combining morphological, geochemical and geochronological data - the example of carbonate breccia-hosted Melnička Peštera. International Journal of Speleology, 53(2), 169-190. https://doi.org/10.5038/1827-806X.53.2.2509

INTRODUCTION

Hypogene speleogenesis develops where the soluble formation is recharged from below, with dissolution of bedrock related to various mechanisms, and sources of acidity originated at depth (Klimchouk, 2007; Palmer, 2007). Recent advances in the understanding of hypogene karst systems led to an increased recognition of hypogene cave occurrences throughout the world (Klimchouk et al., 2017), and inspired further research interest in the field. Most of the cave development in hypogene karst occurs under confined hydrogeological settings at depth (Klimchouk, 2007). However, our understanding of these systems is largely based on the study of fossil caves, that became accessible only after being intercepted by surface erosion (Klimchouk

*temovski.marjan@atomki.hu

et al., 2017). In such settings, much of the primary hypogene features might be removed or overprinted by epigene processes (e.g., Columbu et al., 2021).

In hydrothermal hypogene karst systems, cave development occurs along the rising limb of the groundwater by cooling CO_2-rich waters due to the retrograde solubility of calcite, and is superseded by calcite deposition in shallower settings due to CO_2 degassing (Dublyansky, 2013). Hypogene caves can develop also near the water table. This is typical for sulfuric acid caves that develop where H_2S-rich deep groundwater interacts with shallow oxygen-rich waters producing sulfuric acid that dissolves the carbonate bedrock (e.g., De Waele et al., 2024). Significant development of cave volume can occur also above the water table by condensation corrosion either by sulfuric or carbonic acid, especially in hydrothermal systems (Audra et al., 2007; De Waele et al., 2016). A single hypogene system can also experience several phases of development during its evolution, starting with initial cave development in deeper settings, that after uplift and/or incision can evolve further near the water table by sulfuric acid speleogenesis and/or condensation corrosion (e.g., Temovski et al., 2013; Columbu et al., 2021).

Hypogene caves can have passages arranged as network mazes, ramiform and spongework patterns, controlled by the dominant porosity type in the soluble formation, ranging from fractures, bedding partings to intergranular porosity, respectively (Palmer, 1991). They can develop in various lithologies, with some of the more notable ones found in limestone (e.g., Carlsbad Caverns, Hill, 1987; Frasassi Caves, Galdenzi & Menichetti, 1995; caves in Buda Hills, Leél-Őssy, 2017) and gypsum (e.g., caves in Western Ukraine, Andreychouk & Klimchouk, 2017). However, hypogene caves have been described also in other lithologies, such as dolomite (e.g., Spötl et al., 2016), quartzite (e.g., Sauro et al., 2014), magnesite (e.g., Bella & Gaal, 2017).

Karst caves can develop also in carbonate conglomerate and detrital breccia deposits, mostly related to epigene speleogenesis, with examples described worldwide (e.g., Degirmeci et al., 1994; Bergada et al., 1997; Ferrarese & Sauro, 2005; Goeppert et al., 2011; Lipar & Ferk, 2011). While the most widespread application of cosmogenic radionuclide (CRN) burial age dating to caves is the estimation of burial duration of trapped allochthonous sediments (e.g., Häuselmann et al., 2005, 2020; Wagner et al., 2010; Bella et al., 2019; Temovski et al., 2024), quartz fragments present in bedrock walls of caves developed in clastic carbonate rocks offer the possibility to determine the CRN burial age of the host-rock formation (e.g., Mihevc et al., 2015).

In this work, we discuss the hypogene speleogenesis of carbonate breccia-hosted Melnička Peštera, based on new morphological observations and geochemical data from secondary minerals in the cave and the surrounding Melnica hypogene karst area. As the stratigraphy and chronology of the carbonate breccia is not well constrained, we use this opportunity to apply CRN burial age dating to quartz fragments in the cave walls to determine the age of the rock formation, and constrain the geological and geomorphological evolution, and setting for karst development.

Recent work on karst and cave development in the drainage basin of Crna Reka in Macedonia, identified epigene speleogenesis related to Pliocene base level rise due to basin infilling, as well as subsequent Pleistocene incision (Temovski, 2016; Temovski et al., 2016, 2024). A possible influence of the Messinian Salinity Crisis (MSC) on base level lowering at the end of Miocene was also inferred, based on stratigraphic information from Neogene basin sediments, as well as cave morphology and associated sediments (Temovski, 2016; Temovski et al., 2024). Hydrothermal and sulfuric acid hypogene speleogenesis was also identified, related to Neogene-Quaternary extension and volcanic activity, with Melnica area hosting the most important findings (Temovski et al., 2013, 2018, 2021, 2022; Temovski, 2016).

STUDY AREA AND SAMPLING LOCATIONS

Melnička Peštera is located at the Melnica locality in Mariovo (N. Macedonia), on the northern side of the Buturica River, a right tributary to Crna Reka (Fig. 1, Supplementary Fig. S1). The cave is developed in carbonate breccia deposits of the Pešta Hill, at the contact with the underlying dolomite marble formation (Fig. 1; Temovski, 2016).

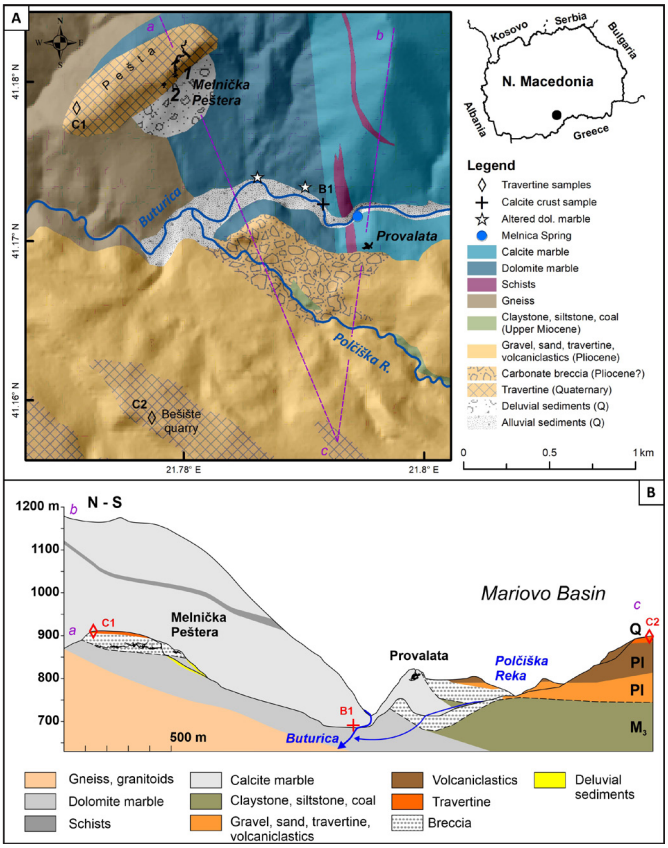

Fig. 1. A - Geological setting of Melnica area, showing cave locations and sampled sites; B - combined geological cross-sections showing the relationship of the breccia deposits and the Mariovo Basin sediments with sampling sites projected relative to stratigraphic position. Wider context of the area is shown in Supplementary Fig. S1. The map and cross-sections are updated from Temovski (2016) based on field observations and borehole data from Gradežen Institut "Makedonija" (2010).

The Melnica area, located along the northern edge of the extensional Mariovo Basin (Supplementary Fig. S1), hosts records of hypogene karst development in both dolomite and calcite marble, with the clearest example in Provalata Cave, where both CO_2-rich hydrothermal and sulfuric acid speleogenesis were identified (Temovski et al., 2013, 2018, 2022). The current activity of this hypogene system is represented by the lukewarm Melnica Spring (Fig. 1), where geochemical data indicates the presence of deep-sourced gases, dominantly CO_2 of metamorphic origin, and mantle helium (Temovski et al., 2021).

Melnička Peštera consists of two caves (Fig. 1), of which Melnička Peštera 1 is much larger with close to 700 m of explored passages (Fig. 2), whereas Melnička Peštera 2 is about 100 m long; the former is the focus of this study. Their passages generally extend horizontally and are covered by numerous convectional solutional pockets in various sizes (Fig. 2). Secondary calcite minerals, appearing as veins or crusts can be seen at many locations in the cave, and appear to predate cave passages (Temovski, 2016; Fig. 3).

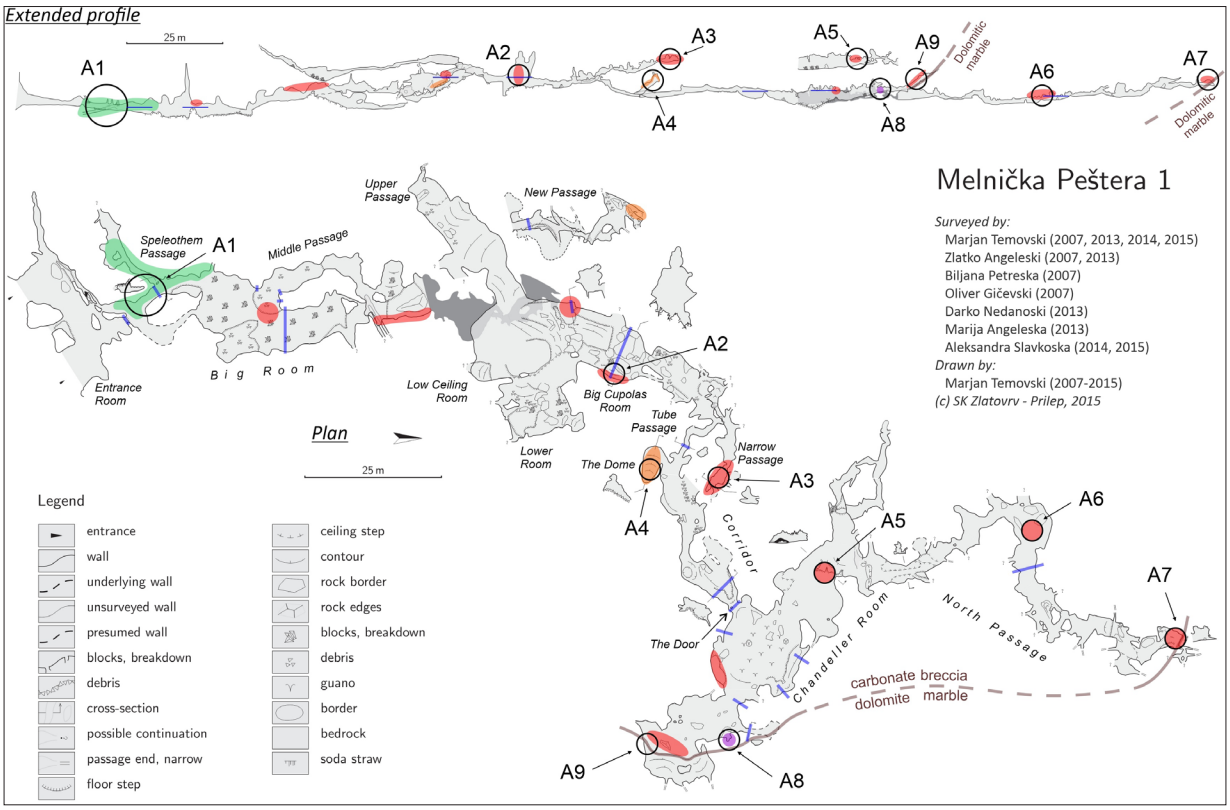

Fig. 2. Cave map of Melnička Peštera 1, updated from Temovski (2016), with sampling locations indicated. Colored shades indicate mapped locations with characteristic secondary cave minerals: red – calcite crust, orange – mammillary-like calcite crust, purple - shelfstone, green – vadose (dripstone) speleothems. Blue lines indicate locations with well-expressed triangular passage cross-sections (Laughöhle) and water-table marks.

Fig. 3. Relationship of calcite crusts with cave morphology in Melnička Peštera 1. A – Convectional features carved in calcite crust in the Narrow Passage (location A3 in Fig. 2); B – Calcite crust lining a solutionally enlarged low angle fracture in the Big Room, cut by subsequent convectional features; C – Two distinct layers of calcite crust filling up cavity in the Chandelier Room (location A5 in Fig. 2). The lower, orange-colored calcite has a gradual transition from the carbonate breccia bedrock, but has a well-expressed convex shape at the boundary with the upper, greyish calcite. They both have been subsequently cut by pockets and cupolas.

Melnička Peštera 1 and 2 are located about 50 m higher and at 1.5 km to the NE from Provalata Cave (Fig. 1). Considering the characteristic small-scale morphology, the proximity to Provalata Cave and identified cave remnants and hydrothermal alterations in Buturica valley between these caves, its origin has been tentatively attributed to hydrothermal speleogenesis (Temovski, 2016).

Sampling was carried out in Melnička Peštera 1 and on the surface in the surroundings of Melnica (Figs 1, 2 and Table 1). At Melnička Peštera 1, secondary cave minerals were collected, for various analyses, at 8 locations, labeled A1 to A8 (Figs 2, 4, Supplementary Fig. S2, Table 1). Vadose dripstone samples were collected near the entrance, at sampling location A1 (Fig. 2, Supplementary Fig. S2). Orange-looking crusts were sampled from: location A2 in the Big Cupolas Room (Figs 2, 4A); the lower layer of the calcite crust at location A5 in the Chandelier Room (Figs 2, 4C, 4E); and at the contact of carbonate breccia and dolomite marble at location A7 (Fig. 2, Supplementary Fig. S2). Greyish-looking crusts were sampled at: location A3 in the Narrow Passage (Figs 2, 4B); the upper layer at location A5 in the Chandelier Room (Figs 2, 4C, 4D); and at location A6 in the Northern Passage (Figs 2, 4F). Additionally, a whitish calcite crust was sampled from mammillary-like coatings in the Dome Room at location A4, and a whitish shelfstone was sampled from a niche in the NE part of the Chandelier Room at location A8 (Fig. 2, Supplementary Fig. S2).

Fig. 4. Sampled secondary calcite minerals in Melnička Peštera. Additional sampling locations are shown in Supplementary Fig. S2. A – Orange-like calcite crust from the Big Room (location A2); B – Greyish calcite crust from the Narrow Passage (location A3); C – Two layers of calcite crust at the ceiling of Chandelier Room (location A5), with close-up of the greyish upper layer shown in D, and the orange-like lower layer in E. F – Greyish calcite crust from the Northern Passage (location A6).

Table. 1. List of sampling locations, collected samples, and performed analyses. Sampling location labels (Figs 1, 2). A – Melnička Peštera, B – Buturica valley unroofed caves; C – Mariovo basin travertines.

Sampling location	No	Collected samples	Sample description	Analyses				
				Conv. stab. iso.	Clumped isotopes	Noble gases in fluid inclusions	U-Th dating	CRN burial dating
A1	1	M2010-16	Soda straw	x	x			
	2	M2401-1	Soda straw	x				
	3	M2401-2	Scratched stalagmite top	x				
A2	4	M2010-17, MEL17-1	Calcite crust	x	x	x	x	
A3	5	M2010-15	Calcite crust	x	x			
	6	MP1-3	Calcite crust	x	x	x	x	
A4	7	M2010-14	Calcite crust (mammillary-like), outer layer	x	x			
A5	8	M2010-8	Calcite crust (lower layer)	x	x			
	9	M2010-7, MEL18-1	Calcite crust (upper layer)	x	x	x	x	
A6	10	M2010-4	Calcite crust	x				
	11	M2010-5	Calcite crust	x				
	12	MP3	Calcite crust	x	x			
A7	13	M2010-01	Quartz fragments (small size)					x
	14	M2010-02	Quartz fragments (large size)					x
	15	M2010-3	Calcite crust at contact with dolomite marble	x	x	x		
A8	16	M2010-13	Shelfstone	x	x		x	
A9	17	M2010-9	Quartz fragments (small size)					x
	18	M2010-10	Quartz fragments (large size)					x
B1	19	M1911-1	Calcite crust	x	x	x	x	
C1	20	M2010-23	Micritic travertine	x	x			
C2	22	M2010-19-1	Crystalline travertine	x	x			
	23	M2010-19-6	Crystalline travertine	x	x			
	24	M2010-19-7	Crystalline travertine	x	x			
	25	M2010-19-9	Micritic travertine	x	x			

At two locations in the cave, at the contact of the breccia hosting the cave and the underlying dolomite marble, quartz fragments within the breccia were sampled for CRN burial age dating of the host rock, to constrain the maximum age of the cave (Figs 2, 5; Table 1).

Secondary calcite minerals were also sampled from Buturica valley, from an unroofed elongated cavity developed along a fracture in dolomite marble (Fig. 1, Supplementary Fig. S3; Table 1). Travertine deposits topping the Mariovo basin sediments were sampled for stable isotope analyses from two locations (Fig. 1, Supplementary Fig. S3; Table 1). From an exposed section at Bešište Quarry, samples were collected from pale yellow, layered, crystalline travertine in the lower and middle parts and pale brown micritic travertine topping the formation. Similar-looking micritic travertine was also sampled at the top of Pešta Hill.

METHODOLOGY

Cave mapping and morphological analyses

The cave map was updated from a previous version (Temovski, 2016), based on additional detailed field mapping in 1:100 scale using Leica laser distance meter (Disto D3) and Suunto compass (Suunto KB-20). Field data (sketches, measurements) were later

processed in Therion cave mapping software (Budaj & Mudrak, 2008). A detailed cave map produced in plan and profile views (Fig. 2), as well as cross-sections showing characteristic morphological features were used for morphological analyses, accompanied by field observations and photographic documentation.

Stable isotope analyses of carbonate

Conventional stable and clumped isotope analyses of carbonates were carried out at the Isotope Climatology and Environmental Research Centre (ICER), HUN-REN Institute for Nuclear Research (ATOMKI), Debrecen, Hungary.

Conventional carbon and oxygen stable isotope analyses were carried out on hand-drilled carbonate powders with an automated GASBENCH II sample preparation device (phosphoric acid digestion at 72°C) attached to a Thermo Scientific Delta V isotope ratio mass spectrometer (IRMS). The results are expressed as $\delta^{18}O_{cc}$ and $\delta^{13}C_{cc}$ values relative to Vienna Pee-Dee Belemnite (VPDB). The precision of the measurements is ≤0.08‰ for $\delta^{13}C$ and ≤0.1‰ for $\delta^{18}O$.

Clumped isotope analysis was carried out on a Thermo Scientific 253 Plus IRMS, after phosphoric acid digestion at 70°C using a Thermo Scientific Kiel IV automatic carbonate device, following the methodology of Meckler et al. (2014) . Each measurement consists of 11-12 replicate analyses of 100-120 µg aliquots, measured alongside normalization standards (ETH-1, ETH-2, and ETH-3), and a monitoring standard (IAEA-C2), following a fully carbonate-based standardization scheme (Bernasconi et al., 2021). The long-term reproducibility of the instrument based on IAEA-C2 measurements varies between 0.025 – 0.033‰. Negative background was corrected by using the pressure-sensitive baseline (PBL) correction of Bernasconi et al. (2013), implemented in the Easotope software (John & Bowen, 2016). The clumped isotope composition of carbonate minerals is expressed as Δ_{47} presented on the I-CDES90°C scale (Bernasconi et al., 2021) without applying an acid fractionation correction factor. Apparent temperatures in °C were calculated based on the Δ_{47}-temperature calibration from Anderson et al. (2021), with temperature uncertainties propagated from the standard error of the Δ_{47} value, as well as from the uncertainty of the calibration equation. During clumped isotope analysis the conventional carbonate stable isotope composition is measured simultaneously with results expressed as $\delta^{18}O_{cc}$ and $\delta^{13}C_{cc}$ values relative to VPDB.

Noble gases

Noble gas isotope analyses of calcite-hosted fluid inclusions were carried out at the ICER, ATOMKI.

For noble gas isotope analyses, 0.8 to 1.9 g of calcite samples were loaded into stainless-steel holders with a magnetic ball and baked at ~60°C for 10–12 h in vacuum before the measurements. Gas was extracted by single-step crushing (~100 strokes) at room temperature (22°C). The relatively low number of strokes was applied for each measurement in order to avoid significant contribution of an in-situ component. Helium isotope abundances and ratios were determined by a HELIX- SFT mass spectrometer, whereas a VG-5400 mass spectrometer was used for neon. The analytical procedures are described in more detail in Papp et al. (2012) and Molnár et al. (2021).

Stratigraphic analysis of the cave-hosting breccia

We examined the stratigraphic position of the cave-hosting carbonate breccia within the Mariovo Basin sediments using published geological data, observations from the cave and surface exposed outcrops in Melnica, as well as borehole data from exploration work related to the coal deposits hosted in the Upper Miocene sediments (Gradežen Institut "Makedonija", 2010).

Geochronology

CRN Burial age dating

Burial dating of sediments relies on radioactive decay of cosmogenic radionuclides (CRN) ^{26}Al and ^{10}Be. During their pre-burial history, quartz-bearing surface sediments accumulate cosmogenic nuclides in an amount roughly inversely proportional to the source denudation rate but at a constant $^{26}Al/^{10}Be$ ratio (Granger & Muzikar, 2001). After their deposition, buried under tens of meters of rock, the CRN production stops, and the burial duration can be calculated using the decrease of the ratio of the two nuclides due to their differential decay constant (Dunai, 2010; Granger, 2006, 2014).

For burial age dating, quartz fragments were collected from the breccia bedrock in Melnička Peštera 1 at the contact with the underlying dolomite marble at two locations, A7 and A9, located at 37 ± 2 m and 25 ± 2 m below the surface, respectively (Table 1, Supplementary Table S1, Fig. 5). At each sampled location two sets of samples were collected, one with ~10 quartz fragments with larger grain size (5-10 cm), and one with ~20-40 quartz fragments with smaller grain size (1-5 cm). The collected rock fragments were amalgamated for each sample, crushed, sieved and the 0.5-1 mm grain size fraction was used for age determination.

Sample processing was performed at the Cosmogenic Nuclide Sample Preparation Laboratory of the Institute for Geological and Geochemical Research (Budapest, Hungary), following the procedures of Merchel & Herpers, (1999) and Merchel et al. (2019) as described in Ruszkiczay-Rüdiger et al. (2021). The stable ^{27}Al was determined using Microwave Plasma – Atom Emission Spectrometry (Agilent 4100 MP-AES) at ATOMKI. AMS (Accelerator Mass Spectrometry) measurements of the isotopic ratios of the samples were carried out at the Vienna Environmental Research Accelerator (VERA), Faculty of Physics, University of Vienna, Austria, as described in Temovski et al. (2024), and in the Supplementary information.

Burial ages were calculated as simple burial ages, considering complete burial, using the equation of Granger & Muzikar (2001), and considering post-burial CRN production at sample subsurface depth, based on inverse modelling (Pappu et al., 2011; Lebatard et al., 2014; Ruszkiczay-Rüdiger et al., 2018). The later enables the estimation of the source

and sink denudation rates together with the burial age, using the equation of Braucher et al. (2011). Sample location data is available in the Supplementary Table S1. Constants and variables used for the age calculations are given in Table 2. CosmoCalc add-in for Excel (Vermeesch, 2007) has been used to convert sample elevations to atmospheric pressures and to calculate the scaled production rate.

Table 2. Parameters used for CRN burial ages calculations (qtz: quartz; SLHL: sea level high latitude).

Parameter/unit	Value	Reference
^{10}Be spallogenic production rate SLHL [atoms/g_{qtz}/y]	4.01 ± 0.33	Borchers et al. (2016)
Scaling of muogenic production rates	Heisinger et al. (2002a, b) modified by Balco (2017), calculated using the code of Nørgaard et al. (2023)	
Attenuation lengths (neutrons, thermal muons, fast muons) [g/cm^2]	160, 1500, 4320	Heisinger et al. (2002a,b); Braucher et al. (2011)
Scaling of spallogenic production rates	time independent	Lal (1991)/Stone (2000); calculated using Vermeesch (2007)
^{10}Be half-life [y]	1 387 000 ± 12 000	Chmeleff et al. (2010); Korschinek et al. (2010)
^{26}Al half-life [y]	705 000 ± 17 000	Nishiizumi (2004)
production rate ratio ^{26}Al/^{10}Be	6.7 ± 0.6	Fenton et al. (2022)
Sediment density after burial [g/cm^3]	2.6	estimated value
Rock density in catchment [g/cm^3]	2.6	estimated value

U-Th dating of calcite

U-Th dating (Edwards et al., 1987; Dorale et al., 2007; Cheng et al., 2013) was carried out on 5 samples from the secondary calcite minerals (Table 1). Sample powders were drilled using a Dremel handheld drill. About 10 mg of carbonate powder was first collected for determination of U concentration on an Agilent 8800 Triple Quadrupole ICP-MS. Based on the U concentration, between 5 and 200 mg of carbonate powder was then collected for U-Th dating.

Chemical preparation to separate U and Th fractions from the carbonate matrix was carried out in a Class 1000 clean laboratory, with procedures similar to those described in Edwards et al. (1987). The isotope ratio measurements were carried out on a Neptune PLUS multicollector ICP mass spectrometer equipped with an Aridus 3 desolvating system. Further details on the analytical procedures are described in Temovski et al. (2024). All preparation procedures and analyses were carried out at ICER, ATOMKI. The U-Th ages were calculated by iteration using the standard ^{230}Th/^{238}U equation (Kaufman & Broecker, 1965; Edwards et al., 1987).

RESULTS

Sedimentary characteristics and stratigraphic position of the carbonate breccia

The carbonate breccia hosting Melnička Peštera is not well described in the geological literature. As it is topped by lacustrine travertine at Pešta hill, it is not reported in the available publications (Dumurdžanov & Hristov, 1976; Dumurdžanov et al. 1976, 2003; Dumurdžanov et al., 2004; unpublished geological maps in 1:25000 scale, Geological Survey Skopje), and is mapped either as part of the travertine deposits, considered to be of Pleistocene age, or the clastic Mariovo basin sediments, assigned to Pliocene. The breccia at Pešta hill was first described as part of the study of the karst and caves in Mariovo (Temovski, 2016).

As observed in Melnička Peštera cave walls, the clast-supported breccia is poorly sorted and polymictic, containing dominantly carbonate rock fragments of various sizes (from few cm up to 1 m, but usually 5-20 cm). Both dolomite and calcite marble fragments can be found, with a small percent of non-carbonate rocks such as gneiss, schist, and quartz fragments. The carbonate fragments are rounded to angular, while the non-carbonate fragments are less rounded, especially the quartz fragments. At places, some marly and sandy layers can be found. A non-carbonate fine-grained fraction can also be present in the matrix, and the formation is carbonate cemented, thus acting as a solid carbonate rock. The thickness of the formation at Pešta hill, that grades upward to travertine deposits, is mostly 30-40 m, up to 50 m (Temovski, 2016).

The same carbonate breccia, with generally smaller fragment sizes, can also be seen at the junction of Buturica and Polčiška valleys (Figs 1 and 5). These sediments are exposed by river incision and also by some quarrying on the western side. Towards the east they overlay the dolomite marble formation.

The breccia deposits have been identified also by recent borehole drilling related to the coal seams in the Upper Miocene formation (Gradežen Institut "Makedonija", 2010). Borehole data also identifies a valley-like depression nested within the Upper Miocene sediments, filled mostly with the breccia deposits, and other Mariovo Basin clastic sediments considered to be of Pliocene age. This depression deepens in the downstream direction and becomes shallower in the upstream part, indicating regressive erosion (Fig. 1).

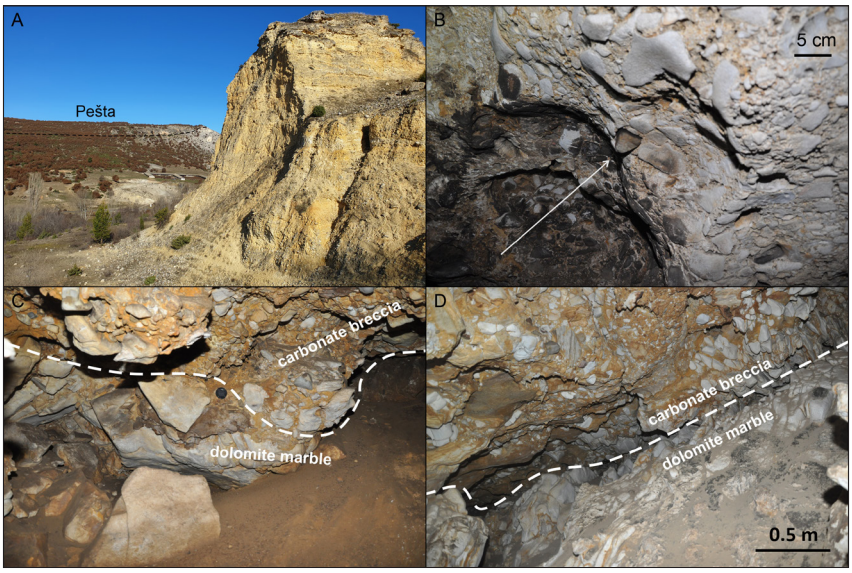

Fig. 5. Characteristics of the carbonate breccia deposits. A - View of the exposed breccia profile in a quarry at the confluence of Buturica and Polčiška Reka. Pešta hill is visible in the back with outlined breccia deposits; B - Solutional features carved in carbonate breccia in Melnička Peštera. Note the smooth wall surface carved in carbonate fragments and the quartz fragment pointing outward from it; C and D – Contact of the carbonate breccia and the underlying dolomite marble in Melnička Peštera at locations A7 (C) and A9 (D), where samples of quartz fragments were collected for burial age dating.

Morphological characteristics of Melnička Peštera

Melnička Peštera has a maze-like pattern of passages, with some sections having spongework and/or ramiform patterns, although its pattern is largely obscured by later collapses (Fig. 2). The vertical extension of the cave is about 17 m, where at least 3 levels of cave passages can be identified (Fig. 2). The cave combines larger cave rooms, with higher ceilings, having spongework-like morphology that contain prominent breakdown, and smaller passages joining them, that due to the current penetrable size gives an impression of main conduit-like passages. However, at closer observation, remnants of sponge-like morphology with numerous pockets and cupolas near breakdown suggest that the cave passages were originally composed of a dense network of interconnected voids, in a spongework-like pattern.

At many places the walls have smooth surfaces, with convectional features (e.g., cupolas, solutional pockets) carved in both the carbonate fragments and the matrix material. Fragments of calcite marble have a smoother appearance than the dolomite marble ones, while the non-carbonate fragments are not corroded and project outward from the wall (e.g., Fig. 5B).

At several places, passage cross-sections have a reverse triangle shape, i.e., characteristic widening in the top part with sides sloping downwards, and ceilings that are flat or extend upwards into cupolas or due to collapse (Fig. 6). Such passage morphology is known as Laughöhle, with flat ceilings termed Laugdecke, or solutional bevels, and the sides, sloping down at near 45° angle, termed facets (Kempe, 1975; Palmer, 2007).

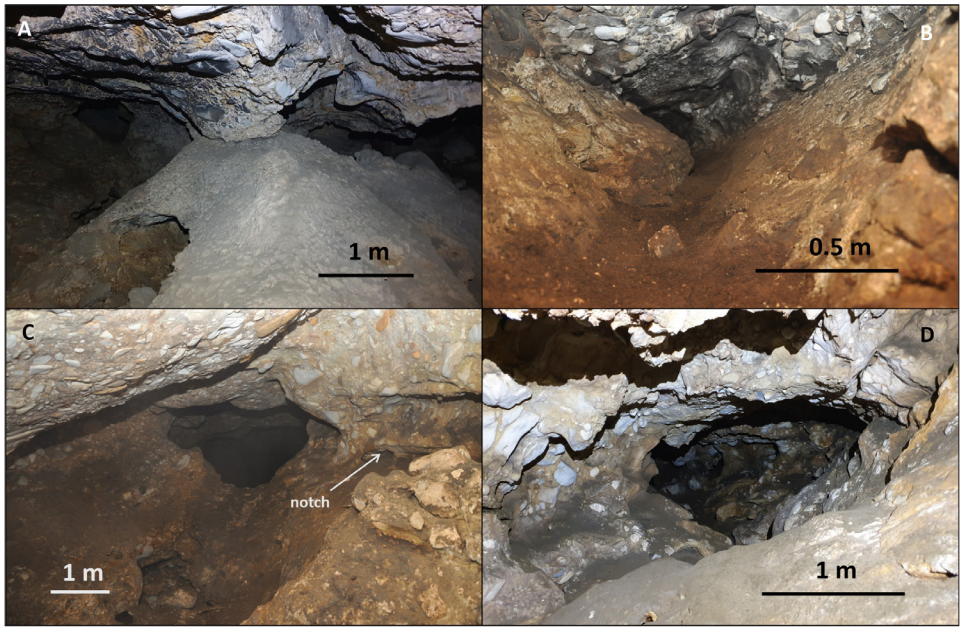

Fig. 6. Triangular shaped passage cross-sections in Melnička Peštera 1. A – in the Big Room; B – Tube Passage; C – The “Door” at the end part of the Corridor. Close-view of the indicated horizontal notch is shown in Figs 7A; D – Side passage in the Chandelier Room close to the contact with the underlying dolomite.

In the larger rooms (e.g., Big Room, Chandelier Room; Figs 2, 7B, and 7C), facets can be found at several levels along the walls, with ceilings, largely affected by breakdown, having remnants of flat sections. In the Northern Passage, Laughöhle morphology is preserved in wider sections with low ceilings (e.g., near sampling location A6; Figs. 2 and 7).

A well-expressed horizontal notch is present on both side walls of the passage at the NE end of the Corridor Passage, just before it joins the Chandelier Room (Figs. 2, 7A). At approximately the same elevation in a niche on the northern side of the Chandelier Room, a shelfstone can be found, extending few cm from the wall (Fig. 2, Supplementary Fig. S2).

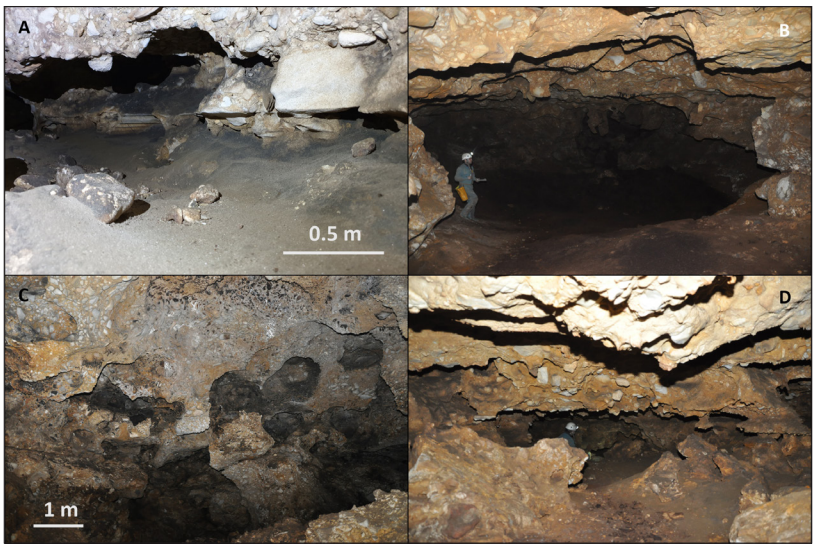

Fig. 7. Morphological indicators of passage development near the water table. A– water table notches at the NE end of the Corridor Passage, just before it joins the Chandelier Room. Note also the wall niches above the notch; B – flat ceilings in the Chandelier Room, cut by ceiling cupolas and pockets. Note the downward sloping facets at the passage walls; C – two generations of facets in the upper parts of the eastern side of the Big Room, with collapsed ceiling morphology hosting cupolas with traces of former bat colonies (black patches); D – flat ceiling above prominent horizontal notch in the Northern Passage (sampling location A6). The proximal part is largely altered by collapses.

Calcite crusts are found at many locations in the cave (Fig. 2), covering solutionally enlarged fractures or cavities with unclear geometry. At many places they are cut by the cave passage, or more commonly cut by smaller scale convectional forms (i.e., cupolas, pockets; Fig. 3), indicating that they pre-date the cave passages.

Convectional features such as cupolas, wall niches and pockets are the most common features found throughout the cave (Fig. 8). They are mostly developed in carbonate breccia, but they can be found cutting through the calcite crust deposits as well. Their origin is most likely related to condensation corrosion above the water table, as they overprint previous forms, such as flat ceilings (Fig. 7B). The wall niches found just above the water table notches in the Corridor Passage, just before the Chandelier Room, clearly support the subaerial origin of these small-scale features (Fig. 7A). The larger volume passages (e.g., Big Room, Chandelier Room) have large collapsed blocks with similar small-scale morphology, reflecting a former dense network of voids. Pendants can be found at a number of places protruding from cave walls and ceilings as remnants between cupolas and solutional pockets. Best expressed are the “Chandeliers” in the Chandelier Room, which have a stacked concave morphology (Fig. 8).

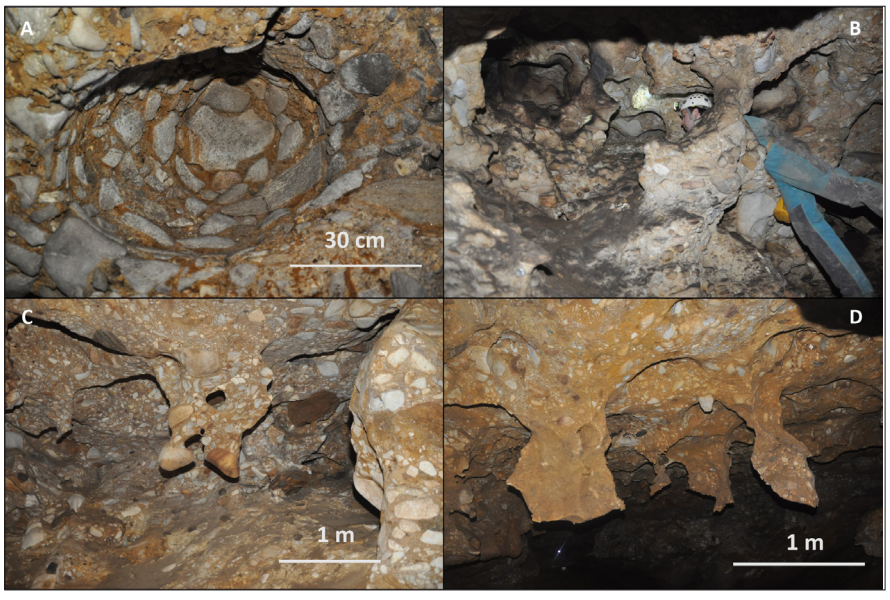

Fig. 8. Characteristic small-scale morphology. A – Cupola in the Big Room; B – Spongework morphology at the lower part of the Narrow Passage; C–D – Pendants at the ceiling of the Chandelier Room.

Some of the ceiling convectional features are likely formed by bat-related biocorrosion (e.g., Audra et al., 2016; Barriquand et al., 2021; Merino et al., 2022). Traces of bat presence can be seen at many locations, with black coatings at the edges of cupolas (Fig. 9A) and yellow-brown coatings on bedrock or highly corroded calcite crusts, likely representing bat-related mineralization (e.g., Audra et al., 2019). Most typical examples can be seen in the Big Cupolas room, the Chandelier Room and the Northern Passage (at sampling location A6). The cave currently hosts a large bat colony, mostly nesting in the Chandelier Room, where thick guano deposits can also be found (Fig. 9).

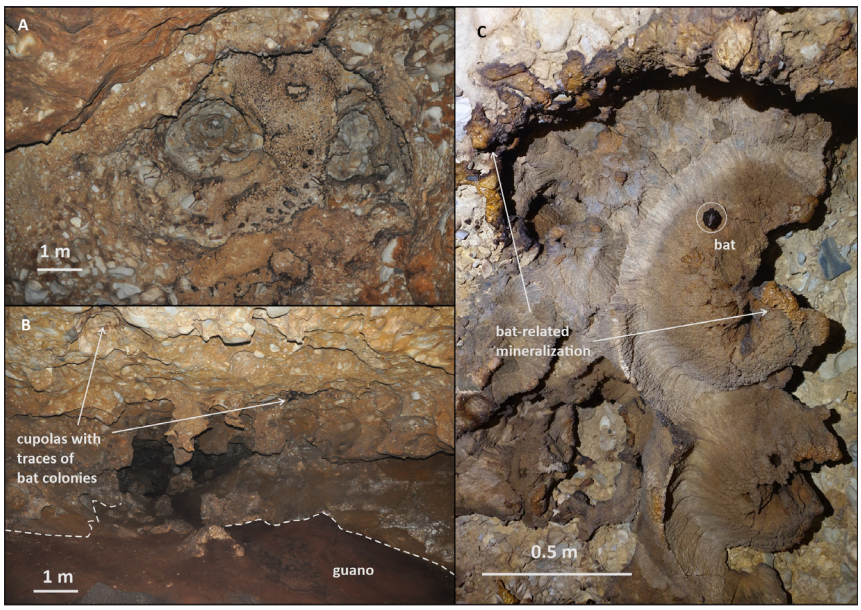

Fig. 9. Bat-related morphological features. A – large cupolas with traces of bat colonies at the ceiling of Big Cupolas Room; B – View of the central part of the Chandelier Room, with floor covered by thick guano deposits, and traces of bat colonies seen in cupolas on the ceiling. Presently, a large bat colony is observed in this part of the cave; C – Highly corroded calcite crusts in the Northern Passage (location A6), partly covered by yellow coatings, likely phosphate minerals.

Stable isotopes

Stable isotope analyses were conducted on a total of 94 subsamples. Of this, 77 were analyzed solely for their conventional stable isotope composition, whereas the remaining 17 were analyzed for both their conventional and clumped isotope composition (Figs 10 and 11; Supplementary Table S4).

The vadose speleothems from Melnička Peštera had generally higher $\delta^{18}O_{cc}$ and lower $\delta^{13}C_{cc}$ values, showing a positive trend with high slope (cluster IV in Fig. 10). The calcite crust samples showed isotopic composition that can be separated in three main clusters.

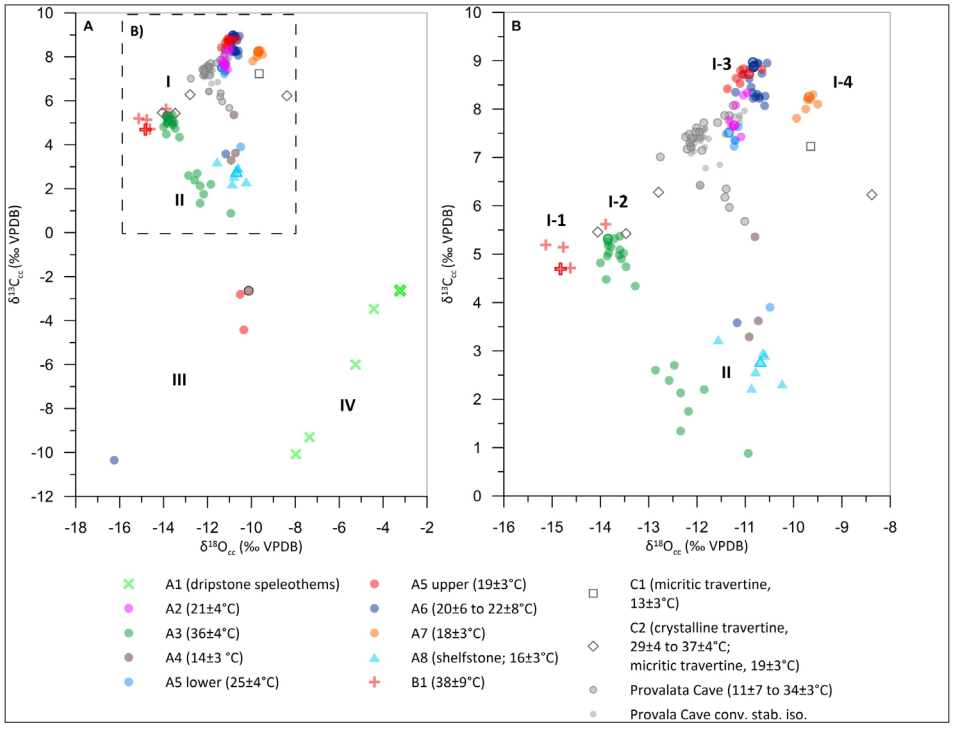

Fig. 10. A - Stable isotope composition of secondary calcite minerals from Melnica hypogene karst area. Thicker outlined color symbols indicate subsamples with available clumped isotope data. Identified clusters and groups are indicated by Roman and Arabic numerals, respectively. Provalata Cave data (Temovski et al., 2022) are also shown for comparison; B - is enlargement of dashed square in A.

The majority of the samples belong to the first cluster (I in Fig. 10) that follows a generally positive trend of $\delta^{18}O_{cc}$ and $\delta^{13}C_{cc}$ values. Four groups can be identified in this cluster. The samples from the unroofed section at location B1 in Buturica Valley (group I-1 in Fig. 10) have the lowest $\delta^{18}O_{cc}$ and $\delta^{13}C_{cc}$ values. Similar $\delta^{13}C_{cc}$ values, with slightly higher $\delta^{18}O_{cc}$ values are found at location A3 in Melnička Peštera (group I-2 in Fig. 10). The next two groups have much higher $\delta^{18}O_{cc}$and $\delta^{13}C_{cc}$ values. The third group includes samples from locations A2, A5 and A6. They have values that partly overlap, with the highest $\delta^{13}C_{cc}$ values found at locality A6 (group I-3 in Fig. 10). Within this group, samples from location A2 are closer to the isotopic composition of the lower layer at A5, while the upper layer at A5 shows similar composition to the samples from location A6. The fourth group in this cluster is represented by the samples from the calcite crust at the contact with dolomite marble at location A7, that has the highest $\delta^{18}O_{cc}$ values of the studied calcite crusts (group I-4 in Fig. 10). The calcite crust from location A4 had one stable isotope data point that can also be placed within this cluster.

The second cluster has lower $\delta^{13}C_{cc}$ values, with a roughly similar trend compared to the first clusters (cluster II in Fig. 10). The shelfstone samples belong to this cluster, that includes also samples from the calcite crusts at location A3, A4, A6 and the lower layer at location A5, that show an obvious shift from their stable isotope profiles (Supplementary Figs S4 – S6).

The third cluster (III in Fig. 10) includes several stable isotope data points that have larger shifts from the stable isotope profiles of samples at locations A4, A6 and the upper layer at A5 (Supplementary Figs S4 – S6).

The travertine samples have a distinct stable isotope composition according to their petrographic characteristics. Crystalline travertine samples had values similar to the calcite crusts, and the micritic travertine samples had higher values, particularly for $\delta^{18}O_{cc}$ (Fig. 10).

The clumped isotope composition showed Δ_{47} values between 0.559 ± 0.021‰ and 0.630 ± 0.007‰, reflecting apparent temperatures from 13 ± 3°C to 38 ± 9°C (Fig. 11). Unaltered calcite crust samples from the first cluster in Melnička Peštera, had apparent temperatures between 18 ± 3°C (location A7) and 36 ± 4°C (location A3). The Buturica valley sample (B1) gave the highest apparent temperature of all studied samples, albeit with high uncertainty (38 ± 9°C). The shelfstone sample (location A8) had a lower apparent temperature of 16 ± 3°C. The calcite crust sample from location A4, that belongs to the third cluster, had apparent temperature of 14 ± 3°C. The soda straw sample, that had the highest $\delta^{18}O$ values, had apparent temperature of 20 ± 3°C. The clumped isotope composition of the travertine samples also followed their petrographic characteristics, with lowest apparent temperatures in the micritic travertine (13 ± 3°C to 19 ± 3°C), and highest in the crystalline travertine (29 ± 4°C to 37 ± 4°C).

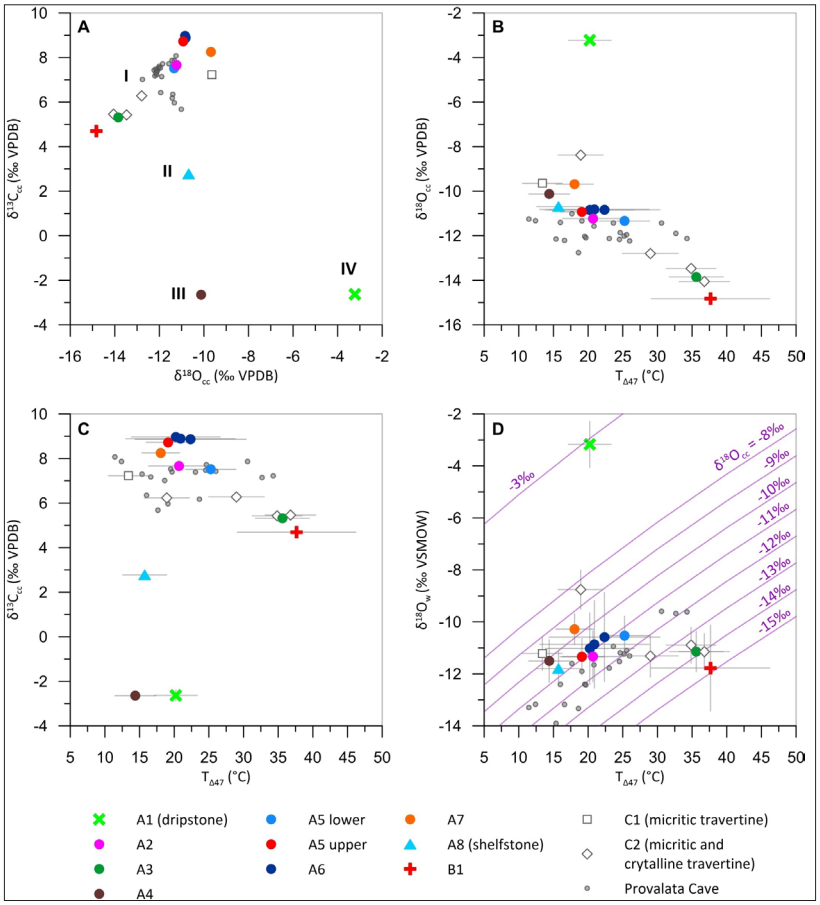

Fig. 11. Stable isotope composition vs clumped isotope-based apparent temperatures and calculated paleofluid $\delta^{18}O_w$ values. Provalata Cave data (Temovski et al., 2022) is shown for comparison. A – $\delta^{18}O_{cc}$ vs $\delta^{13}C_{cc}$ plot showing stable isotope composition of samples with available clumped isotope data. Roman numerals show clusters from Fig. 10. B – Clumped isotope-based apparent temperature ($T_{\Delta47}$) vs $\delta^{18}O_{cc}$ values. C - $T_{\Delta47}$ vs $\delta^{13}C_{cc}$ values. D - $T_{\Delta47}$ vs calculated paleofluid $\delta^{18}O_w$ values. Purple lines show calcite equilibrium lines for a given $\delta^{18}O_{cc}$ based on the equation of Daëron et al. (2019). The soda straw sample (A1) is likely affected by kinetic effects, shifting its isotopic composition to higher $\delta^{18}O_{cc}$ and $\delta^{13}C_{cc}$ values, and lower Δ_{47} values (higher apparent temperature).

Using the calcite-water oxygen equilibrium equation of Daëron et al. (2019), and based on the measured $\delta^{18}O_{cc}$ and the clumped isotope-based apparent temperature, we calculated the paleowater oxygen isotope composition ($\delta^{18}O_w$; Supplementary Table S4). Except for the soda straw sample that had much higher $\delta^{18}O_w$ value (-3.2‰), the calculated values for the other samples ranged between -11.8‰ and -8.8‰ $\delta^{18}O_w$. The calcite crust and shelfstone samples had a much narrower range of values, between -11.8‰ and -10.3‰ $\delta^{18}O_w$. The crystalline travertine had low $\delta^{18}O_w$ values (-11.3‰ to -11.1‰), with the micritic travertine between -11.2‰ and 8.8‰.

Except for the soda straw sample, the studied samples showed a clear negative trend between their apparent temperatures and oxygen isotope composition (Fig. 11), indicating that the temperature is the main control on their $\delta^{18}O_{cc}$ values. A similar trend can be seen between the apparent temperature and $\delta^{13}C_{cc}$ values of the samples belonging to the first cluster.

Noble gases

Fluid inclusion noble gas composition was analyzed in five samples: four from Melnička Peštera and one from location B1 in Buturica Valley. Measured He concentrations are 0.7-64.0×10^{-9} ccSTP/g_{cc} and neon concentrations are 0.02-18.60×10^{-9} ccSTP/g_{cc} (Fig. 11; Supplementary Table S3). Helium isotope ratios (R = ^{3}He/^{4}He) ranged from 0.11 to 3.41 R/R_A (where R_A is the atmospheric ratio with value of 1.384×10^{-6}; Sano et al., 2013), with ^{4}He/^{20}Ne ratios from 1.2 to 30.8. The sample from the upper layer at location A5 (MEL18-1; Supplementary Table S3) had the highest R/RA value, albeit with a very low He concentration, close to the measurement blank levels (0.1-0.3×10^{-9} ccSTP/g_{cc}). At such low concentration, its noble gas isotopic composition has to be considered cautiously. This subsample was collected close to the contact with the lower layer, and as the stable isotope composition of the samples near the contact between these layers indicates subsequent alteration (Supplementary Fig. S4), this sample was excluded from further calculation.

Based on a three-end-member mixing model of atmospheric- (R/R_A = 1, ^{4}He/^{20}Ne = 0.318), crustal- (R/R_A = 0.02, ^{4}He/^{20}Ne = 1000) and MORB mantle- (R/R_A = 8; ^{4}He/^{20}Ne = 1000) sourced helium and neon (Sano & Wakita, 1985; Sano & Marty, 1995; Graham, 2002), crustal helium is the dominant component (64-98%) in the studied samples, with mantle helium from 1-11% and atmospheric helium from 1-27% (Fig. 12; Supplementary Table S1). The sample from Buturica Valley (location B1) as well as A3 at Melnička Peštera had the lowest atmospheric helium (1%). The former showed almost pure crustal helium signature, while the one from A3 had 10% mantle helium. The other two samples from Melnička Peštera had high atmospheric helium content, although with a different mantle helium component, that was higher at A2 (11%) and lower at A7 (3%).

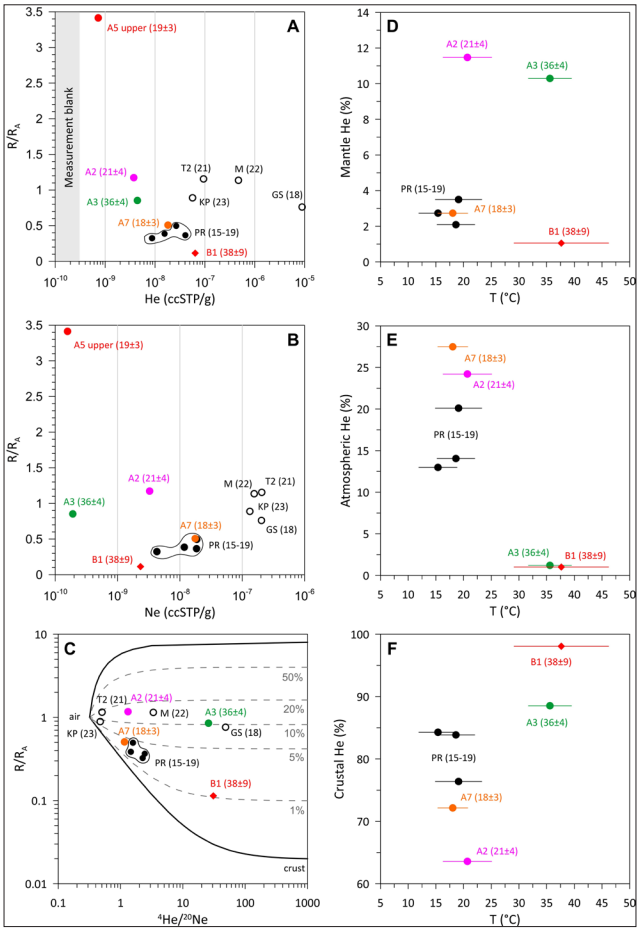

Fig. 12. Noble gas data from the studied calcite samples and their comparison to formation temperatures. Also included are data from fluid inclusions of Provalata Cave calcite (Temovski et al., 2022) and lukewarm springs in Mariovo (Temovski et al., 2021). Studied samples are labeled according to sampling location as listed in Table 1. PR – Provalata Cave calcite; M – Melnica Spring; KP – Karši Podot Cave; GS – Gudjakovo Springs; T2 – Toplek 2 Spring. Calcite formation temperatures (based on clumped isotopes) or measured spring temperatures are given in parenthesis in °C. Sample A5 upper is excluded from graphs in C-F.

CRN Burial age of the carbonate breccia

Laboratory data and measurement results are provided in Supplementary Table S2. The blank corrected ^{10}Be concentrations varied between (15.12 ± 1.27)×10^3 at/g$_{quartz}$ and (62.86 ± 2.17)×10^3 at/g$_{quartz}$. The blank corrected ^{26}Al concentrations varied between (38.50 ± 4.37)×10^3 at/g$_{quartz}$ and (71.43 ± 5.52)×10^3 at/g$_{quartz}$. The reported analytical uncertainties comprise the 1σ confidence level of the AMS measurements and laboratory uncertainties (weighing, carrier concentration, blank correction). The burial ages are discussed throughout the text with their external uncertainties. These include the analytical uncertainties and the uncertainty of the half-lives of ^{10}Be and ^{26}Al, of the spallogenic production rate of ^{10}Be, of the ^{26}Al/^{10}Be spallogenic production rate ratio and of the sample depth.

The ^{26}Al/^{10}B ratios of the samples were 1.1 ± 0.2 and 1.4 ± 0.1 for the samples at the deeper, A7 location and 2.5 ± 0.4 and 2.0 ± 0.3 at the A9 sample site at shallower subsurface depth (Supplementary Table S2). The simple burial age, assuming complete burial and spallogenic CRN production only, was estimated at 3.67 ± 0.55 Ma and 3.29 ± 0.48 Ma for the location A7, and at 2.00 ± 0.38 Ma and 2.46 ± 0.44 Ma for location A9 (Table 3). These ages can be considered as minimum burial ages, as post-burial CRN production at the sampled depth is not accounted for.

The burial age considering the subsurface depth of the samples and all production pathways was 4.21 ± 0.67 Ma and 3.78 ± 0.59 Ma for A7 location, and 4.63 ± 0.95 Ma and 4.74 ± 0.92 Ma for A9. Post-burial CRN production has a major effect at shallower subsurface depth and on samples of smaller CRN concentrations (M2010-09 and M2010-10; sampling location A9), resulting in an increase of the decay-controlled ^{26}Al/^{10}B ratio and a larger increase of the most probable or true burial age compared to the minimum burial age (Supplementary Table S2 and Table 3). This explains why the true burial age of the samples at the A7 location have increased by 13% while those at the A9 location by ~50% when the post-burial CRN production at the sample depth was accounted for (Table 3). The true ages overlap within uncertainties, and constrain the age of the carbonate breccia between 4.74 ± 0.92 and 3.78 ± 0.59 Ma, with a weighted mean age of 4.19 ± 0.37 Ma.

Table 3. Calculated CRN burial ages of the samples, as minimum burial ages (A) considering complete burial, and most probable burial ages (B), considering post-burial CRN production at subsurface sample depth.

Burial age calculation	Sample location	Sample	Burial age (Ma)	Internal uncertainty (Ma)*	External uncertainty (Ma)**	Sink denudation rate (m/Ma)	Internal uncertainty (Ma)*	External uncertainty (Ma)**	Source denudation rate (m/Ma)	Ext. uncertainty (m/Ma)**
A	A7	M2010-01	3.67	0.31	0.55	n.a.	n.a.	n.a.	n.a.	n.a.
		M2010-02	3.29	0.25	0.48	n.a.	n.a.	n.a.	n.a.	n.a.
	A9	M2010-09	2.00	0.28	0.38	n.a.	n.a.	n.a.	n.a.	n.a.
		M2010-10	2.46	0.31	0.44	n.a.	n.a.	n.a.	n.a.	n.a.
B	A7	M2010-01	4.21	0.41	0.67	8.4	0.8	1.3	12.6	2.0
		M2010-02	3.78	0.32	0.59	8.4	0.7	1.3	18.1	2.8
	A9	M2010-09	4.63	0.38	0.95	19.8	1.6	4.1	67.3	13.8
		M2010-10	4.74	0.33	0.92	19.8	1.4	3.9	40.0	7.8
	Mean		4.34	0.36	0.78	-	-	-	-	-
	Weighted mean		4.19	-	0.37	-	-	-	-	-

*analytical uncertainties only; **analytical, half-lives and SLHL production rate of ^{10}Be and ^{26}Al/^{10}Be production rate ratio uncertainties.

U-series results

U-series measurements were carried out on four samples from Melnička Peštera and one from Buturica Valley. Except for one sample from Melnička Peštera that was shelfstone (from sampling location A8; Tables 1, 4), the remaining ones were calcite crusts. No ages could be resolved from infinity for three samples (from locations A3, A8 and B1), suggesting they are older than 650 ka. However, their δ^{234}U and ^{230}Th/^{238}U values are different than 0‰ and 1, respectively, which are the values for secular equilibrium in well preserved, unaltered calcite, indicating that these samples are younger than 2.5 Ma. Two samples gave U-Th ages of 338 ± 42 ka (A2) and 141 ± 11 ka (lower layer at A5).

DISCUSSION

Formation, age and geomorphological setting of the carbonate breccia

The difference between the clast size of the carbonate breccia deposits in Melnička Peštera (with larger boulders) and the bottom of the valley (generally small size), as well as their geometry, indicate a fan-like depositional setting. The wide Ramnobor paleovalley, which developed in marble and gneiss rock formations, fed this alluvial fan that developed at the junction with the main paleovalley cut into the Upper Miocene sediments of the Mariovo Basin. CRN burial age dating suggests active development of the alluvial fan between ~4.7 ± 0.9 Ma and ~3.8 ± 0.6

Ma, with a weighted mean age of 4.2 ± 0.4 Ma. The obtained Early Pliocene age of the breccia constrains the possible age for the incision of the paleovalley in the Upper Miocene sediments. The incision of this valley might be due to regressive erosion related to the offshore effect of the MSC. The MSC (5.96-5.33 Ma; Krijgsman et al., 1999) caused desiccation of the Mediterranean Sea, that lowered the base level, and forced tributary rivers to cut deep valleys (Bache et al., 2012). A depositional hiatus at the end of Miocene has been reported for many of the Macedonian basins, including the Mariovo Basin (Dumurdzanov et al., 2004, 2005). Evidence of a possible MSC influence on the landscape evolution was identified in the wider region, with Miocene erosional surfaces and Pliocene Gilbert-type deltas identified in the present Vardar drainage in Macedonia (e.g., Clauzon et al., 2008; Suc et al., 2015), but also indirectly in the development of karst systems in the downstream parts of the Crna Reka drainage (Temovski, 2016; Temovski et al., 2024).

Table 4. U-series results.

Location	Subsample	Material	^{238}U (ppb)	^{232}Th (ppt)	$^{230}Th/^{232}Th$ (atomic x10^{-6})	$\delta^{234}U_m$	$^{230}Th/^{238}U$ (activity)	Age uncorr. (ka BP)	$\delta^{234}U_{in}$	Age corr. (ka BP)
A2	M2010-17	Calcite crust	6.7 ± 0	3583 ± 20	31.4 ± 0.2	36.1 ± 13	1.0074 ± 0.0057	353 ± 48	93.6 ± 35.7	338 ± 42
A3	MP1-3-B-01	Calcite crust	59.5 ± 0.1	15721 ± 141	63 ± 0.8	7.5 ± 3.1	1.0092 ± 0.0088	>650		
A5	M2010-7	Calcite crust (lower layer)	4 ± 0	2033 ± 11	27.4 ± 0.3	90.1 ± 14	0.8409 ± 0.0071	155 ± 6	134.3 ± 21.3	141 ± 11
A8	M2010-13-B-01	Shelfstone	440.1 ± 0.6	25517 ± 250	289.7 ± 3.7	12.1 ± 3.7	1.0179 ± 0.0085	>650		
B1	M1911-C-01	Calcite crust	3537.2 ± 5.4	30591 ± 72	1900.2 ± 6.6	-2.9 ± 2.5	0.9963 ± 0.0029	>650		

In the center of the paleovalley, the breccia deposits mixed with siliciclastic sediments and are covered by volcaniclastic sediments (Fig. 1). The Pliocene sediments in Mariovo Basin are assigned to two formations (Dumurdžanov et al., 2003, Dumurdzanov et al., 2004): Solnje and Vitačevo. The Solnje Fm. (sand, gravel and silty clay) is in lower stratigraphic position and lacks volcaniclastic sediments, while the Vitačevo Fm. grades gradually from it and includes various clastic sediments, travertine layers, volcanic tuff and agglomerates. Preliminary geochronological results from the pyroclastics in Mariovo Basin indicate 3.8-3.6 Ma for the volcaniclastics near Vitolište, east of the study area (Supplementary Fig. S1; Molnár et al., 2022a). This correlates well with the burial age of the carbonate breccia, and indicates that coeval infilling of Mariovo Basin paleovalleys at Melnica occurred in the Pliocene. The Ramnobor paleovalley to the north (Supplementary Fig. S1) provided mainly carbonate fragments deposited in an alluvial-fan-like setting, while clastic (non-carbonate) and dominantly volcaniclastic sediments were sourced from the east, related to the activity of the Kožuf volcanic system (Molnár et al., 2022b).

Secondary calcite deposits in Melnička Peštera and Melnica hypogene karst

Most of the studied calcite crusts have high $\delta^{13}C_{cc}$ values, between +4 and +9‰, and follow mostly a positive trend in their $\delta^{18}O_{cc}$ and $\delta^{13}C_{cc}$ values (Fig. 13). Calcite crusts from nearby Provalata Cave (Temovski et al., 2022), fall in the middle of this trend. Some samples also fall on a less prominent negative trend, perpendicular to the first one. Combined fluid inclusion and carbonate stable isotope analyses of the Provalata Cave calcite indicated isotopic equilibrium for their oxygen isotopes (Temovski et al., 2022). If the carbon isotope composition during calcite precipitation was affected by kinetic effects, the oxygen isotope composition would have been affected as well. Thus, kinetic effects for the high $\delta^{13}C_{cc}$ values of the calcite crusts from both caves can be excluded. The insight from Provalata calcite showed that the positive trend in the $\delta^{18}O_{cc}$ and $\delta^{13}C_{cc}$ values resulted from combined effects of temperature and CO_2 degassing from high pCO_2 waters, with cooling leading to increased values of both $\delta^{18}O_{cc}$ and $\delta^{13}C_{cc}$. The negative trend in $\delta^{18}O_{cc}$ and $\delta^{13}C_{cc}$ values indicates deposition from waters with a decrease in pCO_2. In both cases, the calcite precipitated from water that had dissolved inorganic carbon (DIC) with high $\delta^{13}C$, reflecting a deep metamorphic CO_2 source (Temovski et al., 2022). For the present Melnica Spring, it has been estimated that up to 54% of the carbon in the DIC is from metamorphic CO_2 with $\delta^{13}C$ of +4.5‰ (Temovski et al. 2021).

The samples with available both conventional and clumped stable isotope data and noble gas data, including the Provalata Cave samples, fall into two sets in their combined noble gas and apparent temperature values (Fig. 12): one with higher mantle helium contribution (10-11%) and another with low mantle helium contribution (1-4%). In both sets, the samples with higher temperature have almost no atmospheric helium, and represent deeper groundwater, while the lower temperature ones show up to 27% atmospheric helium, and reflect increased contribution of shallow groundwater. Both sets show a similarly large range in their $\delta^{13}C_{cc}$ values with a general increase in $\delta^{13}C_{cc}$with decrease in temperature, and an increase in atmospheric helium.

A similar trend of $\delta^{13}C_{cc}$ and $\delta^{18}O_{cc}$ with decreasing temperature can be observed for almost all of the Melnička Peštera samples (Figs. 10), except for

the shelfstone and the dripstone. The lower carbon isotope composition and apparent temperature of the shelfstone likely reflects conditions when the cave was close to the water table.

The vadose samples also have positive relationship between their $\delta^{18}O_{cc}$ and $\delta^{13}C_{cc}$ values although with higher slope. Positive trends in $\delta^{18}O_{cc}$ and $\delta^{13}C_{cc}$ for vadose speleothems generally indicates kinetic effects during calcite precipitation (Hendy, 1971). This is also supported by the high $\delta^{18}O_{cc}$ and $\delta^{13}C_{cc}$ values for the soda straw sample with clumped isotope data, as well as its high apparent temperature, with kinetic effects generally shifting the clumped isotope composition to lower Δ_{47} values (Affek et al., 2008; Daëron et al., 2011).

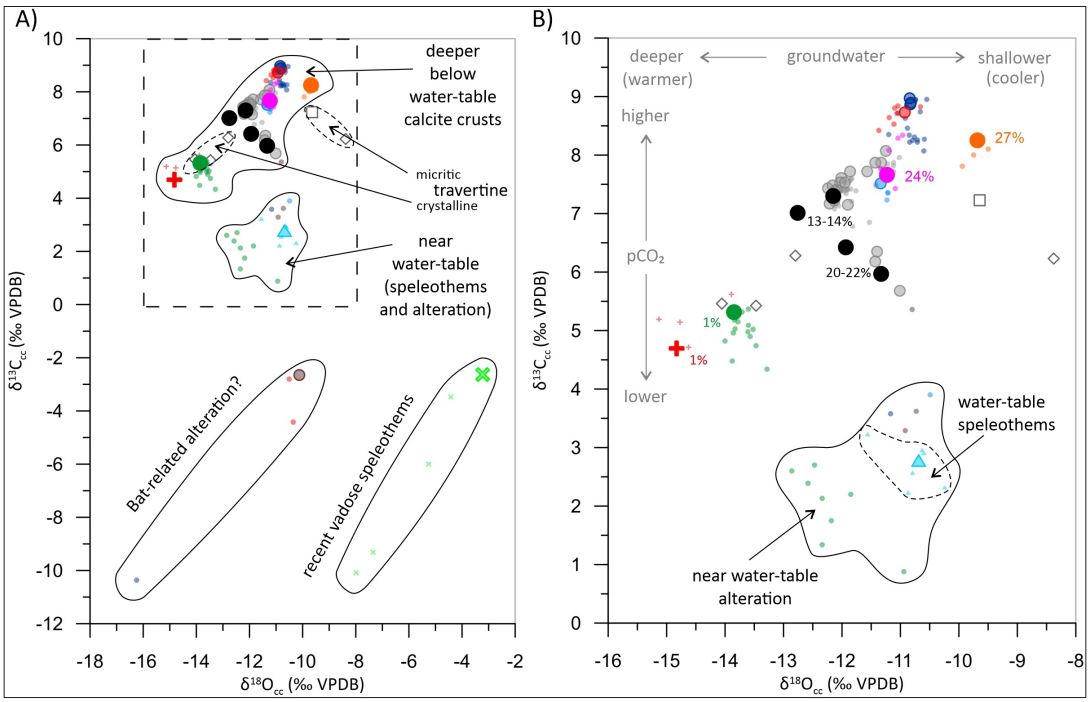

Fig. 13. A - Interpretation of the formation conditions for the hydrothermal calcite in the Melnica hypogene karst. Larger symbols with indicated percen-tage values show the atmospheric helium component in studied fluid inclusions; B - Close-up view of the dashed square in A. For symbol legend, see Figs 10 and 11.

A number of subsamples from the studied calcite crusts at Melnička Peštera, generally towards the outer surfaces of the crusts, had values that appear shifted to lower $\delta^{13}C_{cc}$ and slightly higher $\delta^{18}O_{cc}$. They cluster around the isotopic composition of the shelfstone, and probably reflect subsequent water-rock interaction with groundwater near the water table.

Several subsamples in the studied crusts had stable isotope values shifted much lower, with $\delta^{13}C_{cc}$ values similar to the vadose speleothems and indicating organic sourced carbon. Patches of black to yellowish coatings were observed covering calcite coatings and bedrock at locations with observable present or former bat presence, likely representing bat-related mineralization (Audra et al., 2019). For some of these stable isotope shifts (e.g., at sample location A6), it is very likely that they were caused by interaction with bat-related fluids.

The U-series data from three of the studied crusts, although not allowing precise dating, suggest that the calcite crusts at Melnička Peštera and Buturica Valley are likely of Early Pleistocene age, similar to the calcite in Provalata Cave (Temovski et al., 2022). This is also in agreement with the mean CRN burial age of ~4.2 ± 0.4 Ma for the breccia bedrock. Two samples gave surprisingly young U-Th ages. For one of them (lower layer at A5), this is likely the result of subsequent alteration, as indicated by the shift in stable isotope composition (Supplementary Fig. S4), and very low noble gas concentrations (Supplementary Table S3; Fig. 12). For the other one (A2), although no alteration was observed in the studied stable isotope profile, similar situation is possible, considering that the crust was subsequently dissolved and currently found only as patches on the cave wall (Fig. 4A).

The relative chronology of the calcite crust deposition can be partly explained by their stratigraphic relationship and geochemical data (Fig. 14). It is reasonable to assume a decrease in age with decrease in temperature, as it also reflects an increase in shallower, cooler water. However, as the calcite samples from Provalata Cave show (Temovski et al., 2022), there can be additional pulses of higher temperature registered along the growth length of the calcite crusts. Such pulse of higher groundwater temperature, may result in a shift in the depositional zone to a shallower setting, and this might explain the several generations of calcite crusts found at Melnička Peštera. The sample at A3 location is located at the highest elevation, and has the highest formation temperature, low atmospheric helium and high mantle helium, and likely represents the oldest phase of hydrothermal calcite deposition in the Melnica hypogene karst system. The remaining ones are all located at a similar elevation. A2 sample has similar mantle helium, but lower temperature and higher atmospheric helium than A3. It has a similar stable isotope composition compared to the lower sample at A5, and is probably of similar age. The upper sample at A5 is stratigraphically younger, has similar

isotopic composition as the sample at A6, and likely represents a third generation of calcite deposition. The sample at A7 has the highest atmospheric helium, low mantle helium and low formation temperature, and likely represents the youngest phase of calcite crust deposition in the breccia at Melnička Peštera.

The similar stable isotope composition of the travertine deposits to the calcite crusts found in Melnička Peštera and Provalata Cave, indicate that they are related to the same hydrothermal system (Figs 13 and 14). The crystalline travertine matches closer the values of the calcite crusts, and likely formed at or near the thermal springs, while the lower apparent temperature and higher calculated $\delta^{18}O_w$ values of the micritic travertine likely reflect deposition further away from the spring sites (Fig. 13).

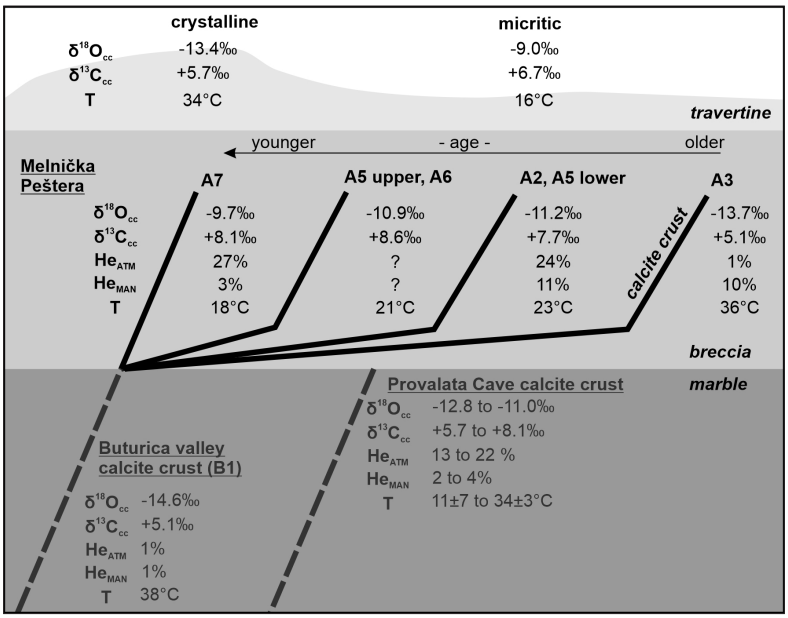

Fig. 14. Schematic illustration of the relative temporal and geochemical evolution of calcite crusts from Melnička Peštera. Data from Buturica Valley calcite crust (B1) and travertine (C1, C2) and Provalata Cave calcite crust (Temovski et al., 2022) are also included. For the stable isotope and T data, average values from unaltered calcite crusts and travertine are given for Melnička Peštera and Buturica valley, and range of values are given for the crusts from Provalata Cave.

Speleogenesis of Melnička Peštera

The relationship between the thermal calcite crusts and the cave passage morphology indicates that the calcite crusts pre-date the horizontal cave passage development. The general horizontal development of the cave, as well as the reverse triangle, Laughöhle passage morphology observed at many cross-sections indicates formation of cave passages near the water-table. Laughöhle morphology has been considered to develop just below the water table, in slow-moving phreatic waters, due to convection as a result of the density difference between undersaturated water in the lower parts of the cavity, and saturated water above due to rock dissolution (Kempe, 1975). Such morphology has been originally described in gypsum caves, but it has been reported also in limestone- (e.g., Spötl et al., 2021; Bela et al., 2022) and dolomite- (e.g., Spötl et al., 2016) hosted caves. However, it has been suggested that it is not clear whether Laughöhle morphology can develop in thermal water, as it is expected for thermally-driven convection to overwhelm the density-driven convection (Dublyansky, 2013). The small-scale convectional morphological features overprinted on cave passages, indicate subsequent development by condensation-corrosion above the water table.

It is difficult to reconcile these observations with a speleogenetic mechanism that can explain their stratigraphic relationship. Deposition of calcite in CO_2-rich hydrothermal systems is constrained to shallower settings, where lower pressure leads to CO_2-degassing and calcite supersaturation. Conversely, at depth, cooling of CO_2-rich hydrothermal waters leads to dissolution (Dublyansky, 2013). In a single system, during its evolutionary path, as it is shifted to shallower settings (due to uplift or erosion), calcite deposits are expected to cover the walls of the previously formed cave passages.

Hypogene cave development at the water table is also characteristic of sulfuric acid speleogenesis, where H_2S-rich fluids react with oxygen-rich shallow waters producing sulfuric acid that develops horizontal passages at the water table and various convectional features by condensation corrosion above the water table (De Waele et al., 2016). Such a situation is found at the nearby Provalata Cave (Fig. 1), where sulfuric acid speleogenesis followed the previous hydrothermal carbonic phase, producing abundant gypsum deposits as a by-product (Temovski et al., 2013, 2018). However, no gypsum deposits were observed at Melnička Peštera. Removal of gypsum deposits by subsequent vadose percolation, as a possible explanation for their absence, is also unlikely, as the cave is very poorly connected to the surface. The small holes in the calcite crust at location A2 in Big Cupolas Room (Fig. 4A), resemble emptied gypsum replacement pockets. However, it is not clear what was the original relationship of the calcite crust and the breccia bedrock at that location, and these holes might be just casts covering rock fragments that were later removed. Some of the observed morphological features, such as wall notches, flat roofs, wall

convection niches, although characteristic of sulfuric acid caves, can be also found in thermal caves that have high CO_2 concentrations due to degassing (De Waele et al., 2016).

Horizontal cave passage development due to mixing of thermal and cold water is also not likely. Autogenic recharge is excluded, as mentioned, due to the poor connection to the surface. Lateral recharge by allogenic waters from the paleo Ramnobor valley is also excluded, as the Laughöhle morphology indicates stagnant or slow flowing waters, and there is no evidence of fluvial sediments.

The horizontal passage development at Melnička Peštera might be related to increased aggressiveness of the low-temperature thermal groundwater near the water table due to high CO_2 concentrations (Fig. 15). CO_2 degassed from the deeper, warmer parts of the aquifer, can reach the water table, partly redissolve in the cooler waters, and escape in the cave atmosphere above the water table. With poor connection to the surface, the concentration of the CO_2 above the water table can greatly increase, and maintain high pCO_2 of the water in contact with it. In such a situation, the highest aggressiveness of the groundwater will be near the water table and will diminish with depth. This can explain the development of a triangular cross-section of the passages close to the water table, as well as the notches at the water table.

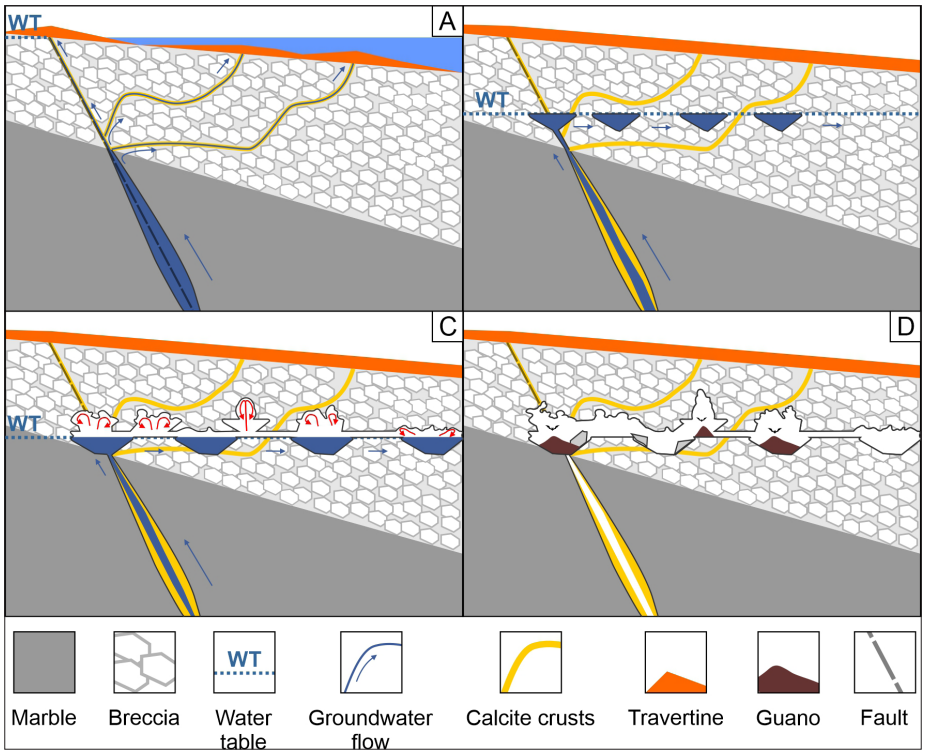

Fig. 15. Schematic representation of the main interpreted speleogenetic phases at Melnička Peštera. A – Circulation of hydrothermal fluids through the breccia deposits along fractures and the primary porosity within the breccia, with deposition of calcite crusts below the surface, and travertine deposits in fluvial to lacustrine environments on surface. Several generations of hydrothermal calcite crusts are formed. At depth dissolution due to cooling of thermal waters creates hypogene cave passages within the marble formation (e.g., nearby Provalata Cave); B – Sealing of the breccia deposits by travertine followed by lowering of the water table, leads to redissolving near the water table of CO_2 previously degassed at depth. This results in increase of solutional capacity of the groundwater near the water table, producing horizontal cave passages with inverted triangle cross-sections, dissolving previously deposited calcite crusts and/or altering their stable isotope composition. At depth, previously formed hydrothermal cave passages are lined by calcite coatings due to degassing of CO_2; C – Horizontal passage development continues at lower elevation due to lowering of the water table, with condensation corrosion above the water table overprinting convective morphological features (e.g., cupolas, ceiling pockets); D – Further lowering of the water table leads to ceiling collapses and subsequent modification by bat-related biocorrosion.

Above the water table, condensation corrosion in a CO_2-rich atmosphere can lead to development of various convectional features, from convection niches just above the water table, to pockets and cupolas higher above it. Such a high pCO_2 environment will also not be favorable for calcite deposition. This is consistent with the observations in the cave, with lack of popcorn deposits that are usually found in such environments in the lower part of the convectional cell, and shelfstone identified only in an isolated niche. The stable isotope composition of the shelfstone shows much lower $\delta^{13}C$ values than the hydrothermal crusts. They are similar to the observed shifts in the altered parts of the studied calcite crusts, indicating that this alteration is due to interaction with the groundwater close to the water table.

The alteration expressed by much lower shifts in $\delta^{13}C$ values observed in some of the samples likely reflects subsequent interaction with bat-related fluids.

Geodynamic setting and evolution of the Melnica hypogene karst – a conceptual synthesis

Governed by the deep incision of the paleo-Crna Reka River at the end of Miocene, its tributary, the paleo-Buturica incised its valley in the Upper Miocene deposits at Melnica. This regressive erosion was likely related to the base level lowering during the MSC. After the base level was restored in the Pliocene, fluvial sedimentation, with mostly angular, carbonate rock-dominated material of variable grain size, occurred in an alluvial fan-like setting at the junction of paleo-Ramnobor and paleo-Buturica

valleys. Concurrently, various clastic and especially volcaniclastic sediments were deposited further away from the alluvial fan, sourced from the upper parts of the drainage of paleo-Buturica River and related to the Kožuf-Voras volcanism.

With continuous filling-up of the valley, the alluvial fan deposits were cemented as carbonate breccia, and cut by fractures related to the extensional evolution of the Mariovo Basin. These fractures were later opened (in Early Pleistocene) by CO_2-rich hydrothermal fluids, that recharged the formation from the underlying marble formations. This led to hydrothermal speleogenesis in the marble formation (e.g., Provalata Cave, alteration in dolomite marble), deposition of calcite crusts in the breccia formation above, and provided the alkalinity for the deposition of travertine at the top of the formation, mostly in lacustrine environments. The onset of the hydrothermal activity at Melnica is likely related to the youngest phase of volcanic activity of the Kožuf-Voras system (3.0-1.8 Ma; Molnár et al., 2022b), as the activity of the volcanic system shifted to the southwest.

The subsequent evolution of the hydrothermal karst system follows general cooling and an increase in the proportion of shallow groundwater. Related uplift caused base level lowering (i.e., draining of the lacustrine system and onset of river incision; Temovski et al., 2013), that shifted calcite deposition downwards (e.g., at Provalata Cave). At least two pulses of increased temperature were registered in Provalata Cave calcite crusts (Temovski et al., 2022), likely related to volcanic events at ~2.5 and ~1.8 Ma (Kolios et al., 1980; Molnár et al., 2022b).

The main cave development at Melnička Peštera occurred when the water table descended to the breccia formation. Phreatic, triangular-shaped passages developed just below the water table due to increased aggressiveness of the groundwater related to recapture of the deep-sourced CO_2 degassed at depth. Notches developed at the contact with the water table, and various conventional features were overprinted on the phreatic morphology by condensation corrosion.

Subsequent base level lowering drained Melnička Peštera, and reached Provalata Cave, where sulfuric acid speleogenesis commenced, mostly by condensation corrosion, and likely related to oxidation of H_2S originating from sulfate reduction in the nearby coal deposits. This resulted in dissolution of marble bedrock and calcite crust and deposition of gypsum as replacement crust, as well as various potassium sulfates at the contact with clay, dated to 1.60-1.46 Ma (Temovski et al., 2013).

The continued incision since Early Pleistocene led to the present situation, where both Provalata Cave and Melnička Peštera are fully drained, but still largely not affected by surface processes. The lukewarm Melnica Spring, located at the Buturica riverbed, represents the active remnant of Melnica hydrothermal karst system.

The horizontal cave development at Melnička Peštera occurred between 2.5 Ma and 1.6 Ma, constrained by the age of the calcite deposition preceding it, and the age of the subsequent sulfuric acid water-table cave development at Provalata Cave. Based on these ages, and considering the location of the cave at 171 m above the current riverbed of Buturica River, the calculated incision rate ranges between 0.07 and 0.11 m/ka, for the last 2.5 and 1.6 Ma, respectively. Similar incision rates, since Early Pleistocene, were obtained for the slightly upstream location at Provalata Cave (~0.06 m/ka), as well as in the upstream part of Kamenica River (0.04 ± 0.01 m/ka), a tributary to Crna Reka in the lower part of the basin (Temovski et al., 2024). Higher incision rates are found in the downstream parts in the Crna Reka basin, with values increasing to ~0.2–0.5 m/ka in Middle Pleistocene, and up to 1 m/ka in Late Pleistocene (Temovski et al., 2016, 2024).

CONCLUSION

Morphological observations in Melnička Peštera suggest development of horizontal cave passages close to the water table by CO_2-rich, likely low temperature thermal waters. The solutional aggressiveness near the water table was likely maintained by redissolved CO_2 that was degassed from the deeper parts of the system, as well as related high pCO_2 in the cave air above the water table, due to poor connection with the surface. The later contributed to development of convectional morphological features by condensation corrosion. Hydrothermal calcite crust deposits, found throughout the cave, pre-date the main phase of cave passage development, and were likely deposited in the Early Pleistocene, similar to the calcite crust in nearby Provalata Cave. Their stable isotope and noble gas composition indicate cooling of the hydrothermal system due to an increased contribution of shallower groundwater. The carbonate breccia formation hosting Melnička Peštera was deposited in an alluvial fan environment in Early Pliocene, at the northern edge of the Mariovo Basin. It filled up a paleovalley cut in Upper Miocene sediments, that likely formed as a result of the base level drop related to the Messinian Salinity Crisis at the end of the Miocene.

ACKNOWLEDGMENT

This research was supported by the National Research, Development and Innovation Office of Hungary grant OTKA FK 124807 and by the European Union and the State of Hungary, co-financed by the European Regional Development Fund in the project of GINOP-2.3.2-15-2016-00009 'ICER'. AMS measurements at Vienna Environmental Research Accelerator, were supported by the RADIATE project under the Grant Agreement 824096 from the EU Research and Innovation programme HORIZON 2020. Fieldwork was carried out under Research Permits Nos. 11-1654/6 issued in 2016 to SK Zlatovrv Prilep by the Ministry of Environment and Physical Planning of the Republic of Macedonia. We thank cavers from SK Zlatovrv Prilep for assistance during fieldwork. We are grateful to Elizabeta Raleva for providing the materials from the Mariovo coal drilling. We are also thankful to Silke Merchel and Peter Steier for their contribution to the AMS measurements. Arthur and Margaret Palmer, Andrea Martín Pérez, and an anonymous reviewer provided valuable comments and recommendations that improved the quality of the manuscript.

Authorship statement: MT designed and directed the study, prepared the figures and wrote the original draft. MT and LR carried out stable isotope analyses. KM and LP carried out noble gas analyses. MT and LP carried out U-Th dating. ZRR, AW and OM carried out burial age dating. All authors contributed to the final version of the manuscript.

REFERENCES

Affek, H.P., Bar-Matthews, M., Ayalon, A., Matthews, A., Eiler, J.M., 2008. Glacial/interglacial temperature variations in Soreq cave speleothems as recorded by "clumped isotope" thermometry. Geochimica et Cosmochimica Acta, 72(22), 5351–5360. https://doi.org/10.1016/j.gca.2008.06.031

Anderson, N.T., Kelson, J.R., Kele, S., Daëron, M., Bonifacie, M., et al. (2021). A unified clumped isotope thermometer calibration (0.5–1,100°C) using carbonate-based standardization. Geophysical Research Letters, 48(7), 1–11. https://doi.org/10.1029/2020GL092069

Andreychouk, V., Klimchouk, A., 2017. Zoloushka Cave (Ukraine–Moldova)—A prime example of hypogene artesian speleogenesis in gypsum. In: Klimchouk, A., Palmer, A.N., De Waele, J., Auler, A.S., Audra, P. (Eds.), Hypogene karst regions and caves of the world. Springer, Cham, 387-406. https://doi.org/10.1007/978-3-319-53348-3_24

Audra, P., Hobléa, F., Bigot, J., Nobecourt, J., 2007. The role of condensation-corrosion in thermal speleogenesis: Study of a hypogenic sulfidic cave in Aix-les-Bains, France. Acta Carsologica, 36(2), 185–194. https://doi.org/10.3986/ac.v36i2.186

Audra, P., Barriquand, L., Bigot, J.-Y., Cailhol, D., Caillaud, H., Vanara, N., Nobécourt, J.-C., 2016. L'impact méconnu des chauves-souris et du guano dans l'évolution morphologique des cavernes. Karstologia, 68, 1-20.

Audra, P., De Waele, J., Bentaleb, I., Chroňáková, A., Krištůfek, V., et al., 2019. Guano-related phosphate-rich minerals in European caves. International Journal of Speleology, 48(1), 75–105. https://doi.org/10.5038/1827-806X.48.1.2252

Bache, F., Popescu, S.M., Rabineau, M., Gorini, C., Suc, J.P., et al., 2012. A two-step process for the reflooding of the Mediterranean after the Messinian Salinity Crisis. Basin Research, 24(2), 125–153. https://doi.org/10.1111/j.1365-2117.2011.00521.x

Balco, G., 2017. Production rate calculations for cosmic-ray-muon-produced ^{10}Be and ^{26}Al benchmarked against geological calibration data. Quaternary Geochronology, 39, 150-173. https://doi.org/10.1016/j.quageo.2017.02.001

Barriquand, L., Bigot, J. Y., Audra, P., Cailhol, D., Gauchon, C., Heresanu, V., Jaillet, S., Vanara, N., 2021. Caves and bats: Morphological impacts and archaeological implications. The Azé Prehistoric Cave (Saône-et-Loire, France). Geomorphology, 388, 107785. https://doi.org/10.1016/j.geomorph.2021.107785

Bella, P., Gaál, Ľ., 2017. Hypogene caves in Slovakia. In: Klimchouk, A., Palmer, A.N., De Waele, J., Auler, A.S., Audra, P. (Eds.), Hypogene karst regions and caves of the world. Cham, 299-312. https://doi.org/10.1007/978-3-319-53348-3_19

Bella, P., Bosák, P., Braucher, R., Pruner, P., Hercman, H., Minár, J., Veselský, M., Holec, J., Léanni, L., 2019. Multi-level Domica–Baradla cave system (Slovakia, Hungary): Middle Pliocene–Pleistocene evolution and implications for the denudation chronology of the Western Carpathians. Geomorphology, 327, 62–79. https://doi.org/10.1016/j.geomorph.2018.10.002

Bella, P., Bosák, P., Pruner, P., Hercman, H., Pukanská, K., Bartoš, K., Gaál, Ľ., Haviarová, D., Tomčík, P., Kdýr, Š., 2022. Speleogenesis in a lens of metamorphosed limestone and ankerite: Ochtiná Aragonite Cave, Slovakia. International Journal of Speleology, 51(1), 13–28. https://doi.org/10.5038/1827-806X.51.1.2397

Bergadà, M.M., Cervello, J.M., Serrat, D., 1997. Karst in conglomerates in Catalonia (Spain): morphological forms and sedimentary sequence types recorded on archaeological sites. Quaternaire, 8, 267–277.

Bernasconi, S.M., Hu, B., Wacker, U., Fiebig, J., Breitenbach, S.F.M., Rutz, T., 2013. Background effects on Faraday collectors in gas source mass spectrometry and implications for clumped isotope measurements. Rapid Communications in Mass Spectrometry, 27, 603-612. https://doi.org/10.1002/rcm.6490

Bernasconi, S. M., Daëron, M., Bergmann, K. D., Bonifacie, M., Meckler, A. N., et al., 2021. InterCarb: A community effort to improve interlaboratory standardization of the carbonate clumped isotope thermometer using carbonate standards. Geochemistry, Geophysics, Geosystems, 22(5), 1–25. https://doi.org/10.1029/2020GC009588

Borchers, B., Marrero, S.M., Balco, G., Caffee, M.W., Goehring, B.M., Lifton, N.A., Nishiizumi, K., Phillips, F.M., Schaefer, J.M., Stone, J.O., 2016. Geological calibration of spallation production rates in the CRONUS-Earth project. Quaternary Geochronology, 31, 188-198. https://doi.org/10.1016/j.quageo.2015.01.009

Braucher, R., Merchel, S., Borgomano, J., Bourles, D.L., 2011. Production of cosmogenic radionuclides at great depth: A multi element approach. Earth and Planetary Science Letters, 309, 1-9. https://doi.org/10.1016/j.epsl.2011.06.036

Budaj, M., Mudrak, S., 2008. Therion—digital cave maps. In: Proceedings of the IV European Speleological Congress, Lans-en-Vercors, France, 33. Spelunca Memoires, p. 138–141.

Cheng, H., Edwards, R.L., Shen, C.-C., Polyak, V.J., Asmerom, Y., et al., 2013. Improvements in ^{230}Th dating, ^{230}Th and ^{234}U half-life values, and U–Th isotopic measurements by multi-collector inductively coupled plasma mass spectrometry. Earth and Planetary Science Letters, 371–372, 82–91. https://doi.org/10.1016/j.epsl.2013.04.006

Chmeleff, J., von Blanckenburg, F., Kossert, K., Jakob, D., 2010. Determination of the ^{10}Be half-life by multicollector ICP-MS and liquid scintillation counting. Nuclear Instruments & Methods in Physics Research, Section B, Beam Interactions with Materials and Atoms, 268, 192–199. https://doi.org/10.1016/j.nimb.2009.09.012

Clauzon, G., Suc, J.-P., Dumurdžanov, N., Melinte-Dobrinescu, M., Zagorchev, I., 2008. The Pliocene Gilbert-type fan delta of Dračevo (Skopje area, Republic of Macedonia). Geologica Macedonica, 2, 21–28.

Columbu, A., Audra, P., Gázquez, F., D'Angeli, I. M., Bigot, J.-Y., et al., 2021. Hypogenic speleogenesis, late stage epigenic overprinting and condensation-corrosion in a complex cave system in relation to landscape evolution (Toirano, Liguria, Italy). Geomorphology, 376, 107561. https://doi.org/10.1016/j.geomorph.2020.107561

Daëron, M., Guo, W., Eiler, J., Genty, D., Blamart, D., Boch, R., Drysdale, R., Maire, R., Wainer, K., Zanchetta, G., 2011. ^{13}C^{18}O clumping in speleothems:

Observations from natural caves and precipitation experiments. Geochimica et Cosmochimica Acta, 75(12), 3303–3317. https://doi.org/10.1016/j.gca.2010.10.032

Daëron, M., Drysdale, R.N., Peral, M., Huyghe, D., Blamart, D., Coplen, T.B., Lartaud, F., Zanchetta, G., 2019. Most Earth-surface calcites precipitate out of isotopic equilibrium. Nature Communications, 10(1), 429. https://doi.org/10.1038/s41467-019-08336-5

De Waele, J., Audra, P., Madonia, G., Vattano, M., Plan, L., D'Angeli, I.M., Bigot, J.-Y., Nobécourt, J.-C., 2016. Sulfuric acid speleogenesis (SAS) close to the water table: examples from southern France, Austria, and Sicily. Geomorphology 253, 452–467. https://doi.org/10.1016/j.geomorph.2015.10.019

De Waele, J., D'Angeli, I. M., Audra, P., Plan, L., Palmer, A. N., 2024. Sulfuric acid caves of the world: A review. Earth-Science Reviews, 250, 104693. https://doi.org/10.1016/j.earscirev.2024.104693

Degirmenci, M., Bayarı, S., Denizman, C., Kurttas, T., 1994. Caves in Conglomerate, Köprüçay Basin (Western Taurids, Turkey). Journal of Caves and Karst Studies, 56, 14–22.

Dorale, J.A., Edwards, R.L., Alexander, E.C., Shen, C.-C., Richards, D.A., Cheng, H., 2007. Uranium-series dating of speleothems: current techniques, limits, and applications. In: Sasowsky, I.D., Mylroie, J.R. (Eds.), Studies of cave sediments. Springer, Dordrecht, 177–197. https://doi.org/10.1007/978-1-4020-5766-3_10

Dublyansky, Y.V., 2013. Karstification by geothermal waters. In: Frumkin, A. (Ed.), Treatise on geomorphology. Academic Press, San Diego, vol. 6, Karst geomorphology, p. 57–71. https://doi.org/10.1016/B978-0-12-374739-6.00110-X

Dumurdžanov, N. Hristov, S., 1976. General Geological map of SFRJ in 1:100 000: sheet Vitolište. Federal Geological Survey, Beograd (in Macedonian).

Dumurdžanov, N., Hristov, S., Pavlovski, B., Ivanova V., 1976. Explanatory notes for the General Geological map of SFRJ: sheets Vitolište and Kajmakčalan. Federal Geological Survey, Beograd, 61 p. (in Macedonian).

Dumurdžanov, N., Krstić, N., Mihajlović, D., Ognjanova-Rumenova, N., Petrov, G., 2003. New data on stratigraphy of the Neogene and Pleistocene in Mariovo, Macedonia. Geologica Macedonica, 17, 43–52.

Dumurdzanov, N., Serafimovski, T., Burchfiel, B.C., 2004. Evolution of the Neogene-Pleistocene basins of Macedonia. Geological Society of America Digital Maps and Charts Series, 1, 20 p.

Dumurdzanov, N., Serafimovski, T., Burchfiel, B.C., 2005. Cenozoic tectonics of Macedonia and its relation to the South Balkan extensional regime. Geosphere, 1, 1–22. https://doi.org/10.1130/GES00006.1

Dunai, T.J., 2010. Cosmogenic nuclides. Principles, concepts and applications in the Earth surface sciences. Cambridge University Press, New York, 187 p.

Edwards, R.L., Chen, J.H., Wasserburg, G.J., 1987. ^{238}U, ^{234}U, ^{230}Th, ^{232}Th systematics and the precise measurement of time over the past 500,000 years. Earth Planetary Science Letters, 81, 175–192. https://doi.org/10.1016/0012-821X(87)90154-3

Fenton, C. R., Binnie, S. A., Dunai, T., Niedermann, S., 2022. The SPICE project: Calibrated cosmogenic ^{26}Al production rates and cross-calibrated $^{26}Al/^{10}Be$, $^{26}Al/^{14}C$, and $^{26}Al/^{21}Ne$ ratios in quartz from the SP basalt flow, AZ, USA. Quaternary Geochronology, 67, 101218. https://doi.org/10.1016/j.quageo.2021.101218

Ferrarese, F., Sauro, U., 2005. The Montello Hill: The "Classical Karst" of the conglomerate rocks. Acta Carsologica, 34(2), 439–448. https://doi.org/10.3986/ac.v34i2.269

Galdenzi, S., Menichetti, M., 1995. Occurrence of hypogenic caves in a karst region: Examples from central Italy. Environmental Geology, 26, 39–47. https://doi.org/10.1007/BF00776030

Goeppert, N., Goldscheider, N., Scholz, H., 2011. Karst geomorphology of carbonatic conglomerates in the Folded Molasse zone of the Northern Alps (Austria/Germany). Geomorphology, 130(3–4), 289–298. https://doi.org/10.1016/j.geomorph.2011.04.011

Gradežen Institute "Makedonija", 2010. Elaborat za izvedeni inženerskogeološki i hidrogeološki istražni i ispituvački raboti vo jaglenovoto naogjalište "Mariovo". Gradežen Institute "Makedonija" A.D., Skopje (in Macedonian).

Graham, D.W., 2002. Noble gas isotope geochemistry of mid-ocean ridge and ocean island basalts: Characterization of mantle source reservoirs. Reviews in Mineralogy and Geochemistry, 47(1), 247–317. https://doi.org/10.2138/rmg.2002.47.8

Granger, D.E., 2006. A review of burial dating methods using ^{26}Al and ^{10}Be. Geological Society of America Special Papers, 415, 1–16. https://doi.org/10.1130/2006.2415(01)

Granger, D.E., 2014. Cosmogenic nuclide burial dating in archaeology and paleoanthropology. In: Holland H.D., Turekian K.K. (Eds.), Treatise on geochemistry, (2nd Ed.), 14, 81-97.

Granger, D.E., Muzikar, P.F., 2001. Dating sediment burial with in situ-produced cosmogenic nuclides: theory, techniques, and limitations. Earth and Planetary Science Letters, 188, 269-281. https://doi.org/10.1016/S0012-821X(01)00309-0

Häuselmann, Ph., Granger, D.E., 2005. Dating of caves by cosmogenic nuclides: method, possibilities, and the Siebenhengste example (Switzerland). Acta Carsologica, 34(1), 43–50. https://doi.org/10.3986/ac.v34i1.278

Häuselmann, P., Plan, L., Pointner, P., Fiebig, M., 2020. Cosmogenic nuclide dating of cave sediments in the Eastern Alps and implications for erosion rates. International Journal of Speleology, 49(2), 107-118. https://doi.org/10.5038/1827-806X.49.2.2303

Heisinger, B., Lal, D., Jull, A.J., Kubik, P.W., Ivy-Ochs, S., Neumaier, S., Knie, K., Lazarev, V., Nolte, E., 2002a. Production of selected cosmogenic radionuclides by muons 1. Fast muons. Earth and Planetary Science Letters, 200, 345-355. https://doi.org/10.1016/S0012-821X(02)00640-4

Heisinger, B., Lal, D., Jull, A.J., Kubik, P., Ivy-Ochs, S., Knie, K., Nolte, E., 2002b. Production of selected cosmogenic radionuclides by muons: 2. Capture of negative muons. Earth and Planetary Science Letters, 200, 357-369. https://doi.org/10.1016/S0012-821X(02)00641-6

Hendy, C.H., 1971. The isotopic geochemistry of speleothems—I. The calculation of the effects of different modes of formation on the isotopic composition of speleothems and their applicability as palaeoclimatic indicators. Geochimica et Cosmochimica Acta, 35(8), 801–824. https://doi.org/10.1016/0016-7037(71)90127-X

Hill, C.A., 1987. Geology of Carlsbad Cavern and Other Caves in the Guadalupe Mountains, New Mexico and Texas. New Mexico Bureau of Mines & Mineral Resources, Bulletin 117, 150 p.

John, C.M., Bowen, D., 2016. Community software for challenging isotope analysis: First applications of 'Easotope' to clumped isotopes. Rapid Communication in Mass Spectrometry, 30, 2285–2300. https://doi.org/10.1002/rcm.7720

Kaufman, A., Broecker, W.S., 1965. Comparison of ^{230}Th and ^{14}C ages for carbonate materials from lakes Lahontan and Bonneville. Journal of Geophysical Research, 70, 4039. https://doi.org/10.1029/JZ070i016p04039

Kempe, S., Brandt, A., Seeger, M., Vladi, F., 1975. "Facetten" and "Laugdecken", the typical morphological elements of caves developing in standing water. Annales de Spéléology, 30, 705–708.

Klimchouk, A.B., 2007. Hypogene speleogenesis: Hydrogeological and morphogenetic perspective. National Cave and Karst Research Institute, Carlsbad, Special Paper 1, 106 p.

Klimchouk, A., Palmer, A.N., De Waele, J., Auler, A.S., Audra, P. (Eds.), 2017. Hypogene karst regions and caves of the world. Cave and karst systems of the world. Springer, Cham., 911 p. https://doi.org/10.1007/978-3-319-53348-3

Kolios, N., Innocenti, F., Manetti, P., Peccerillo, A., Giuliani, O., 1980. The Pliocene volcanism of the Voras Mts (Central Macedonia, Greece). Bulletin of Volcanology, 43, 553–568. https://doi.org/10.1007/BF02597692

Korschinek, G., Bergmaier, A., Faestermann, T., Gerstmann, U.C., Knie, K., et al., 2010. A new value for the half-life of ^{10}Be by heavy-ion elastic recoil detection and liquid scintillation counting. Nuclear Instruments & Methods in Physics Research, Section B, Beam Interactions with Materials and Atoms, 268, 187–191. https://doi.org/10.1016/j.nimb.2009.09.020

Krijgsman, W., Hilgen, F.J., Raffi, I., Sierro, F.J., Wilson, D.S., 1999. Chronology, causes and progression of the Messinian Salinity Crisis. Nature, 400, 652–655. https://doi.org/10.1038/23231

Lal, D., 1991. Cosmic ray labeling of erosion surfaces – In situ nuclide production rates and erosion models. Earth and Planetary Science Letters, 104(2–4), 424–439. https://doi.org/10.1016/0012-821X(91)90220-C

Lebatard, A.E., Alçiçek, M.C., Rochette, P., Khatib, S., Vialet, A., et al., 2014. Dating the *Homo erectus* bearing travertine from Kocabaş (Denizli, Turkey) at at least 1.1 Ma. Earth and Planetary Science Letters, 390, 8–18. https://doi.org/10.1016/j.epsl.2013.12.031

Leél-Őssy, S., 2017. Caves of the Buda Thermal Karst. In: Klimchouk, A., Palmer, A.N., De Waele, J., Auler, A.S., Audra, P. (Eds.), Hypogene karst regions and caves of the world. Springer, Cham, 279-298. https://doi.org/10.1007/978-3-319-53348-3_18

Lipar, M., Ferk, M., 2011. Eogenetic caves in conglomerate: An example from Udin Boršt, Slovenia. International Journal of Speleology, 40(1), 53–64. https://doi.org/10.5038/1827-806X.40.1.7

Meckler, A.N., Ziegler, M., Millán, M.I., Breitenbach, S.F.M., Bernasconi S.M., 2014. Long-term performance of the Kiel carbonate device with a new correction scheme for clumped isotope measurements. Rapid Communication in Mass Spectrometry, 28, 1705-1715. https://doi.org/10.1002/rcm.6949

Merchel, S., Herpers, U., 1999. An update on radiochemical separation techniques for the determination of long-lived radionuclides via accelerator mass spectrometry. Radiochimica Acta, 84, 215-219. https://doi.org/10.1524/ract.1999.84.4.215

Merchel, S., Gärtner, A., Beutner, S., Bookhagen, B., Chabilan, A., 2019. Attempts to understand potential deficiencies in chemical procedures for AMS: Cleaning and dissolving quartz for ^{10}Be and ^{26}Al analysis. Nuclear Instruments and Methods in Physics Research Section B, 455, 293-299. https://doi.org/10.1016/j.nimb.2019.02.007

Merino, A., Fornós, J. J., Mulet, A., Ginés, J., 2022. Guano-derived morphologies and associated minerals in Cova de sa Guitarreta, Llucmajor, Balearic Islands. International Journal of Speleology, 51(1), 43–58. https://doi.org/10.5038/1827-806X.51.1.2410

Mihevc, A., Bavec, M., Häuselmann, P., Fiebig, M., 2015. Dating of the Udin Boršt conglomerate terrace and implication for tectonic uplift in the northern part of the Ljubljana Basin (Slovenia). Acta Carsologica, 44(2), 169–176. https://doi.org/10.3986/ac.v44i2.2033

Molnár, K., Czuppon, G., Palcsu, L., Benkó, Z., Lukács, R., Kis, B.-M., Németh, B., Harangi, S., 2021. Noble gas geochemistry of phenocrysts from the Ciomadul volcanic dome field (Eastern Carpathians). Lithos, 394–395, 106152. https://doi.org/10.1016/j.lithos.2021.106152

Molnár, K., Lahitte, P., Benkó Z., Fellin G.M., Colin M., Szepesi J., Temovski M., 2022a. Plio-Pleistocene activity in the Mariovo basin, N. Macedonia. In: Peytcheva, I., Lazarova, A., Granchovski, G., Ivanova, R., Lakova, I., Metodiev, L. (Eds.). XXII International Congress of the Carpathian-Balkan Geological Association (CBGA): Geologica Balkanica Abstracts, 378.

Molnár, K., Lahitte, P., Dibacto, S., Benkó, Z., Agostini, S., et al., 2022b. The westernmost Late Miocene-Pliocene volcanic activity in the Vardar Zone (North Macedonia). International Journal of Earth Sciences, 111, 749-766. https://doi.org/10.1007/s00531-021-02153-2

Nishiizumi, K., 2004. Preparation of ^{26}Al AMS standards. Nuclear Instruments and Methods in Physics Research, Section B: Beam Interactions with Materials and Atoms, 223–224, 388–392. https://doi.org/10.1016/j.nimb.2004.04.075

Nørgaard, J., Jansen, J.D., Neuhuber, S., Ruszkiczay-Rüdiger, Z., Knudsen, M.F., 2023. P–PINI: A cosmogenic nuclide burial dating method for landscapes undergoing non-steady erosion. Quaternary Geochronology, 74, 101420. https://doi.org/10.1016/j.quageo.2022.101420

Palmer A.N., 1991. Origin and morphology of limestone caves. Geological Society of America Bulletin, 103(1), 1-21. https://doi.org/10.1130/0016-7606(1991)103%3C0001:OAMOLC%3E2.3.CO;2

Palmer, A.N., 2007. Cave geology. Cave Books, Dayton, 454 p.

Papp, L., Palcsu, L., Major, Z., Rinyu, L., Tóth, I., 2012. A mass spectrometric line for tritium analysis of water and noble gas measurements from different water amounts in the range of microlitres and millilitres. Isotopes in Environmental and Health Studies, 48(1), 494–551. https://doi.org/10.1080/10256016.2012.679935

Pappu, S., Gunell, Y., Akhilesh, K., Braucher, R., Taieb, M., Demory, F., Thouveny, N., 2011. Early Pleistocene presence of Acheulian hominins in South India. Science, 331, 1596–1599. https://doi.org/10.1126/science.1200183

Ruszkiczay-Rüdiger, Zs., Csillag, G., Fodor, L., Braucher, R., Novothny, Á., Thamó-Bozsó, E., Virág A., Pazonyi, P., Timár, G., ASTER Team, 2018. Integration of new and revised chronological data to constrain the terrace evolution of the Danube River (Gerecse Hills, Pannonian Basin). Quaternary Geochronology, 48, 148-170. https://doi.org/10.1016/j.quageo.2018.08.003

Ruszkiczay-Rüdiger, Zs., Neuhuber, S., Braucher, R., Lachner, J., Steier, P., Wieser, A., Braun, M., ASTER Team, 2021. Comparison and performance of two cosmogenic nuclide sample preparation procedures of in situ produced ^{10}Be and ^{26}Al. Journal of Radioanalytical and Nuclear Chemistry, 329(3), 1523-1536. https://doi.org/10.1007/s10967-021-07916-4

Sano, Y., Wakita, H., 1985. Geographical distribution of ^{3}He/^{4}He ratios in Japan: implications for arc tectonics and incipient magmatism. Journal of Geophysical Research, 90, 8729–8741. https://doi.org/10.1029/JB090iB10p08729

Sano, Y., Marty, B., 1995. Origin of carbon in fumarolic gas from island arcs. Chemical Geology, 119(1–4), 265–274. https://doi.org/10.1016/0009-2541(94)00097-R

Sano, Y., Marty, B., Burnard, P., 2013. Noble gases in the atmosphere. In: Burnard P (Ed), The noble gases as geochemical tracers. Springer, Berlin, p. 17–31. https://doi.org/10.1007/978-3-642-28836-4_2

Sauro, F., De Waele, J., Onac, B.P., Galli, E., Dublyansky, Y., Baldoni, E., Sanna, L., 2014. Hypogenic speleogenesis in quartzite: the case of Corona 'e Sa Craba Cave (SW Sardinia, Italy). Geomorphology, 211, 77–88. https://doi.org/10.1016/j.geomorph.2013.12.031

Spötl, C., Desch, A., Dublyansky, Y., Plan, L., Mangini, A., 2016. Hypogene speleogenesis in dolomite host rock by CO_2-rich fluids, Kozak Cave (southern Austria). Geomorphology, 255, 39–48. https://doi.org/10.1016/j.geomorph.2015.12.001

Spötl, C., Dublyansky, Y., Koltai, G., Cheng, H., 2021. Hypogene speleogenesis and paragenesis in the Dolomites. Geomorphology, 382, 107667. https://doi.org/10.1016/j.geomorph.2021.107667

Stone, J.O., 2000. Air pressure and cosmogenic isotope production. Journal of Geophysical Research, 105, 23753. https://doi.org/10.1029/2000JB900181

Suc, J.P., Popescu, S.M., Do Couto, D., Clauzon, G., Rubino, J.L., et al., 2015. Marine gateway vs. fluvial stream within the Balkans from 6 to 5 Ma. Marine and Petroleum Geology, 66, 231–245. https://doi.org/10.1016/j.marpetgeo.2015.01.003

Temovski, M., 2016. Evolution of Karst in the Lower Part of Crna Reka River Basin. Springer International Publishing, 265 p. https://doi.org/10.1007/978-3-319-24547-8

Temovski, M., Audra, P., Mihevc, A., Spangenberg, J., Polyak, V., McIntosh, W., Bigot, J.-Y., 2013. Hypogenic origin of Provalata Cave, Republic of Macedonia: a distinct case of successive thermal carbonic and sulfuric acid speleogenesis. International Journal of Speleology, 42(3), 235–246. https://doi.org/10.5038/1827-806X.42.3.7

Temovski, M., Pruner, P., Hercman, H., Bosák, P., 2016. A cave response to environmental changes in the Late Pleistocene: a study of Budimirica Cave sediments, Macedonia. Geologia Croatica, 69(3), 307–316. https://doi.org/10.4154/gc.2016.29

Temovski, M., Futó, I., Túri, M., Palcsu, L., 2018. Sulfur and oxygen isotopes in the gypsum deposits of the Provalata sulfuric acid cave (Macedonia). Geomorphology, 315, 80–90. https://doi.org/10.1016/j.geomorph.2018.05.010

Temovski, M., Túri, M., Futó, I., Braun, M., Molnár, M., Palcsu, L., 2021. Multi-method geochemical characterization of groundwater from a hypogene karst system. Hydrogeology Journal, 29(3), 1129–1152. https://doi.org/10.1007/s10040-020-02293-w

Temovski, M., Rinyu, L., Futó, I., Molnár, K., Túri, M., et al., 2022. Combined use of conventional and clumped carbonate stable isotopes to identify hydrothermal isotopic alteration in cave walls. Scientific Reports, 12(1), 9202. https://doi.org/10.1038/s41598-022-12929-4

Temovski, M., Wieser, A., Marchhart, O., Braun, M., Madarász, B., Kiss, G. I., Palcsu, L., Ruszkiczay-Rüdiger, Z., 2024. Pleistocene valley incision, landscape evolution and inferred tectonic uplift in the central parts of the Balkan Peninsula – Insights from the geochronology of cave deposits in the lower part of Crna Reka basin (N. Macedonia). Geomorphology, 445, 108994. https://doi.org/10.1016/j.geomorph.2023.108994

Vermeesch, P., 2007. CosmoCalc: An Excel add-in for cosmogenic nuclide calculations. Geochemistry, Geophysics, Geosystems, 8, Q08003. https://doi.org/10.1029/2006GC001530

Wagner, T., Fabel, D., Fiebig, M., Häuselmann, P., Sahy, D., Xu, S., Stüwe, K., 2010. Young uplift in the non-glaciated parts of the Eastern Alps. Earth and Planetary Science Letters, 295(1-2), 159-169. https://doi.org/10.1016/j.epsl.2010.03.034